Hindawi
Complexity
Volume 2020, Article ID 5681703, 29 pages
https://doi.org/10.1155/2020/5681703

Research Article

Nonlinear Dynamics and Power Generation on a New Bistable Piezoelectric-Electromagnetic Energy Harvester

Minghui Yao,[1] **Pengfei Liu**,[2] **and Hongbo Wang**[3]

[1]*School of Artificial Intelligence, Tiangong University, Tianjin 300387, China*
[2]*School of Mechanical Engineering, Tiangong University, Tianjin Key Laboratory of Modern Mechatronics Equipment Technology, Tianjin 300387, China*
[3]*College of Mechanical Engineering, Beijing University of Technology, Beijing Key Laboratory of Nonlinear Vibrations and Strength of Mechanical Structures, Beijing 100124, China*

Correspondence should be addressed to Minghui Yao; merry_mingming@163.com

Received 5 January 2020; Revised 5 April 2020; Accepted 29 May 2020; Published 4 September 2020

Guest Editor: Viet-Thanh Pham

Copyright © 2020 Minghui Yao et al. This is an open access article distributed under the Creative Commons Attribution License, which permits unrestricted use, distribution, and reproduction in any medium, provided the original work is properly cited.

This paper focuses power generation and nonlinear dynamic behaviors on a new bistable piezoelectric-electromagnetic energy harvester. Three different kinds of piezoelectric cantilever beam structures, which include the monostable piezoelectric cantilever beam, the bistable piezoelectric cantilever beam with spring and magnet, and the bistable piezoelectric cantilever beam with spring, magnet, and coil, are designed. The power generation efficiency and dynamic behaviors for each structure are experimentally studied, respectively. Due to the spring introduced, the system easily goes through the potential barrier. Experimental results show that the power generation structure of the bistable piezoelectric-electromagnetic harvester can vibrate between two steady states in a wider range of the frequency. Therefore, the effective frequency bandwidth is broadened about 2 Hz when the spring is introduced under the condition of the suitable magnetic distance. Comparing with the power generation efficiency for three different kinds of structures, it is found that the bistable piezoelectric-electromagnetic harvester has the optimum characteristics, which include the optimal magnetic distance of 15 mm, the optimal load of 8 MΩ, and the parameters variation law of coils. For this structure, the influences of the external excitation and the magnetic distance on the output voltage and dynamic behaviors of the system are examined.

1. Introduction

The energy harvesting technology is a way to convert the energy of the environment into electrical energy, for example, solar energy, heat energy, sound energy, wind energy, and vibration energy. Based on much research results, the conversion efficiency of the environmental vibration energy is the best. Therefore, the vibration energy harvester has been widely studied. At present, there are three kinds of the vibration energy harvesters, such as the electrostatic type, the piezoelectric type, and the electromagnetic type. Since the electrostatic type of the energy harvester requires the external power supply and has usually the complex structure, there are few studies. Because the piezoelectric structure and the electromagnetic structure have great harvesting efficiencies and do not need the external power supply, these two structures have been widely investigated. In recent years, scholars have theoretically and experimentally studied the power generation efficiency and dynamic behaviors of the piezoelectric beam structure and the electromagnetic power generation structure. A number of innovative structures have been proposed. The study on energy harvesters of piezoelectric type, electromagnetic type, and piezoelectric-electromagnetic combined type is introduced as follows.

The first type of the vibration energy harvesting is the piezoelectric type, which utilizes the piezoelectric effect of materials to convert the vibration energy of the environment into the electrical energy. The piezoelectric power generation has advantages of the great output voltage, the simple structure, no electromagnetic interference, and no pollution.

The piezoelectric power generation structures do not need the external power supply, so it has been widely investigated. Researchers have designed many kinds of the piezoelectric energy harvesters. Roundy et al. [1] studied a method of power supply for wireless sensor nodes based on low amplitude vibrations. The results of simulations showed that the output power of the piezoelectric structure was obviously great. Leland and Wright [2] designed and tested a vibration energy harvester with the tunable resonance frequency. This structure reduced its resonance frequency by using the novel method of an axially compressing piezoelectric beam. Beeby et al. [3] did a review of the vibration energy harvesting for the wireless and self-powered microsystems applications. There were three main approaches that could be used to capture the vibration energy of the environment. The advantages and disadvantages of each technology were described in this review. Mann and Owens [4] investigated a nonlinear energy harvester, which used magnetic interactions to design a generator with a bistable potential well. Both theoretical and experimental results showed that the potential well-escaped phenomenon broadened the effective frequency bandwidth of the energy harvester. Stanton et al. [5] examined a bistable nonlinear piezoelectric generator, which could respond in a wide range of the frequencies. Erturk and Inman [6] explored the relation between the power generation efficiency and nonlinear vibration of the bistable piezoelectric cantilever beam. They found that the magnetic piezoelectric structure had a larger vibration amplitude and a greater output power than the piezoelectric structure without magnet. Ferrari et al. [7] established a nonlinear energy harvesting system of the single magnet. The experimental results indicated that the bistable motion significantly improved the output voltage and the output power. Ma et al. [8] theoretically and experimentally investigated a magnetic piezoelectric energy harvester. The frequency bandwidth of the magnetic piezoelectric structure was broadened effectively compared with the piezoelectric structure without magnet. Arrieta et al. [9] examined a novel piezoelectric energy harvester with the bistable cantilevered structure. The bistable cantilevered structure enhanced the harvesting efficiency of the system. Al-Ashtari et al. [10] introduced a new design of the energy harvester, which improved the output power without changing the resonance frequency of the structure. The stiffness of the structure was added by the attractive force between two permanent magnets. Theoretical and experimental results showed that the great output power was generated when the piezoelectric cantilever beam only had a slight deformation. Ali and Kyle [11] explored a vibration energy harvester based on a miniature asymmetric air-spaced cantilever beam, which can generate the great power density. It was sufficient to support the electric power of the most wireless sensor nodes. Fan et al. [12] designed a roller to actuate vibration of the piezoelectric beam, which can capture the energy from both sway and bidirectional vibrations. Yao et al. [13] investigated complicated nonlinear dynamic behaviors of the simply supported laminated composite piezoelectric beam subjected to the axial load and the transverse load. Numerical results showed that the periodic motions and the chaotic motions existed in nonlinear vibrations of the system. Jemai et al. [14] studied parameter optimization of a vibration energy harvester by using piezocomposite material and interdigitated electrode. Arkadiusz et al. [15] exploited the snap-through phenomenon between two stable states of a bistable energy harvesting device. Xie and Wang [16] examined a high efficient cylinder composite piezoelectric energy harvester. The newly designed cylinder piezoelectric energy harvester can provide more efficient energy harvesting under a higher dimension and a higher rotating speed of the roller.

The second type of the vibration energy harvesting is the electromagnetic type, which uses Faraday's law of electromagnetic induction to convert the vibration energy of the environment into the electrical energy. The power generation structure of the electromagnetic induction does not require the external power supply. It has been widely used in the field of the power generation. Galchev et al. [17] investigated an electromagnetic vibration power generator, which can efficiently harvest the energy from low-frequency excitations and nonlinear vibrations. Sari et al. [18] examined a wideband electromagnetic vibration generator. The microgenerator generated the stable output power in a wide range of the external excitation frequencies. Mann and Sims [19] experimentally and theoretically investigated a novel energy harvesting device, which used the magnetic levitation to design an oscillator with the tunable resonance frequency. The results showed that the nonlinear phenomenon can be exploited to improve the effectiveness of the energy harvesting devices. Sardini and Serpelloni [20] experimentally studied a nonlinear electromagnetic energy harvester for capturing the vibration energy of the low frequency. The effectiveness of harvesting of the nonlinear structure was greater than that of the linear structure. Zorlu et al. [21] presented a new electromagnetic energy harvester based on vibration, which harvested the energy from low-frequency vibration within a range of 1–10 Hz. The electromagnetic energy harvester with the magnet and the spring was proposed by Foisal et al. [22]. The friction between the magnet and the tube was reduced by using the lubricant in order to improve the output voltage. Ramlan et al. [23] carried out an experimental study to illustrate the dynamic characteristic of the dual mode and the bistable nonlinear energy harvester under the harmonic excitation. The nonlinear device had a greater power generation efficiency than that of the linear device. Kremer and Liu [24] investigated the energy harvester with the nonlinear energy sink. It had the capacity of absorbing the energy in a wide range of frequencies. Seol et al. [25] studied the combined energy harvester with simultaneous triboelectric and electromagnetic power generation. Resali and Salleh [26] investigated the performance of two types of the electromagnetic power generation devices, which one used the wound coil wire and the other used the printed circuit board coil.

The third type of the vibration energy harvesting is the piezoelectric-electromagnetic combined power generation structure. In order to improve the power generation efficiency of the energy harvester, there is a new trend towards simultaneously using the piezoelectric type, the

electromagnetic type, the photovoltaic type, and other energy conversion types. Since the electromechanical coupling coefficient of the electromagnetic and piezoelectric power generation structure is great, the piezoelectric-electromagnetic combined power generation structures are paid more attention. The prospects of the combined power generation devices are valued by many experts. Wacharasindhu and Kwon [27] experimentally dug into a novel microenergy harvester, which can harvest the energy from typing motions on the computer keyboard. Tadesse et al. [28] analyzed a multimode energy harvesting device, which combined electromagnetic and piezoelectric energy harvesting mechanism. The harvesting efficiency of the device was improved in a wide range of the frequencies. Challa et al. [29] studied a coupled piezoelectric-electromagnetic energy harvesting technique for improving the performance of the power generation devices. Karami and Inman [30] proposed a novel combined energy harvester, which used the nonlinear harvesting mechanisms to improve the output power and broaden the frequency bandwidth. A novel piezoelectric and electromagnetic combined energy harvester was investigated by Yang et al. [31]. When the polarization direction of magnets was perpendicular to the plane of coils, coils generated the maximum output voltage. Wang et al. [32] examined a two-degree-of-freedom combined energy harvester based on the piezoelectric and electromagnetic conduction. They concluded that the power generation efficiency of the combined energy harvester was greater than that of the single energy harvester. Mahmoudi et al. [33] validated the enhancement of the performance of a combined nonlinear energy harvester by theoretical investigation, which is based on the piezoelectric and electromagnetic transduction. Hamid and Yuce [34] designed a new wearable energy harvesting system combined piezoelectric and electromagnetic energy harvesters. It harvested the energy from low-frequency vibrations of the human motion. It showed that the combined power generation structure could be applied to the life. Yao et al. [35, 36] studied carefully power generations of the bistable energy harvester with L-shaped piezoelectric cantilever beam.

The piezoelectric power generation structures combined with electromagnetic induction were studied by a few scholars. At present, most of investigations were focused on the monostable piezoelectric-electromagnetic combined power generation structure. There were few investigations on the bistable piezoelectric-electromagnetic combined power generation structures. A multimode vibration generator, which combines the piezoelectric power generation, the electromagnetic power generation, and the bistable structure, is designed. This multimode vibration generator has been applied for the international patent (PCT/CN2015/077888), and the patent has been public. In the next study, the power generation efficiency of the bistable piezoelectric-electromagnetic combined power generation structure is explored, and dynamic behaviors of it are analyzed.

In this paper, the power generation efficiency and dynamic behaviors of the bistable piezoelectric-electromagnetic combined energy harvester based on vibration are mainly studied. The design of both bistable and multimode structure improves the power generation efficiency of the piezoelectric part and the electromagnetic part. The magnet at the end of the spring does the telescopic reciprocating motion in the tube so that the magnetic flux of the coil is constantly changing to induce electromotance. The influence of external excitation frequencies, external excitation amplitudes, magnetic distances, loads, and coils on the power generation efficiency of the bistable piezoelectric-electromagnetic combined power generation structure is explored. Dynamic behaviors of the system under the different external excitation are studied. Comparing with the earlier studies given by Yao et al. [37], this paper is extended to add the analysis of the potential energy for the bistable power generation structure and explore the influences of the magnetic distance, the optimal external load, and coils on the power generation.

2. Experimental Setups

In the experiment, the piezoelectric cantilever beam, coils, magnets, and the spring are fixed on the fixture. The fixture is fixed on the vibration exciter. The signals are sent to the power amplifier by the signal generator to control vibration of the piezoelectric cantilever beam. The displacement of vibration of the piezoelectric cantilever beam is captured by using the high precision laser detector, and the time-displacement data are obtained. Then, data are sent to computer by the LK-G controller. The output voltage of the system is measured by multimeter. Finally, time-displacement data are analyzed by the LK-Navigator and Origin software. The experimental setups include the YE1311 signal generator, the YE5874 power amplifier, the JZK series of the electric vibration exciter, the high precision laser detector, the multimeter, and the LK-Navigator, as shown in Figure 1(a). The experiment fixture and the circuit are shown in Figure 1(b).

3. Experimental Materials

The materials used in the experiment are the piezoelectric beam, coils, resistances, springs, magnets, and wires, as shown in Figure 2. The piezoelectric material used in the experiment is the PVDF. The PVDF material is not easily damaged when the cantilever beam vibrates with a large vibration amplitude. The base layer of the piezoelectric beam is the brass. The PVDF layers and the brass are combined by the conductive adhesive. The length of the piezoelectric beam is 90 mm, the width is 10 mm, and the thickness is 0.51 mm, respectively. The thickness of the PVDF layer is 30 microns. The piezoelectric materials on the upper and lower layers are fully covered. The piezoelectric strain constant is 17 PC/N. The piezoelectric voltage constant is 0.2 Vm/N. The size of the square magnet at the end of the piezoelectric beam is 8 mm × 5 mm × 2 mm. The diameter of the cylindrical magnet at the end of the spring is 10 mm, and the thickness is 8 mm. The coil is the copper wire. The length of the soft spring is 20 mm, and the initial wire diameter of the spring is 0.5 mm. The initial spring stiffness is 1018 N/m, as calculated by the formula $k = (Gd^4/8D^3)$, where k indicates the spring stiffness; G denotes the shear module of the spring and

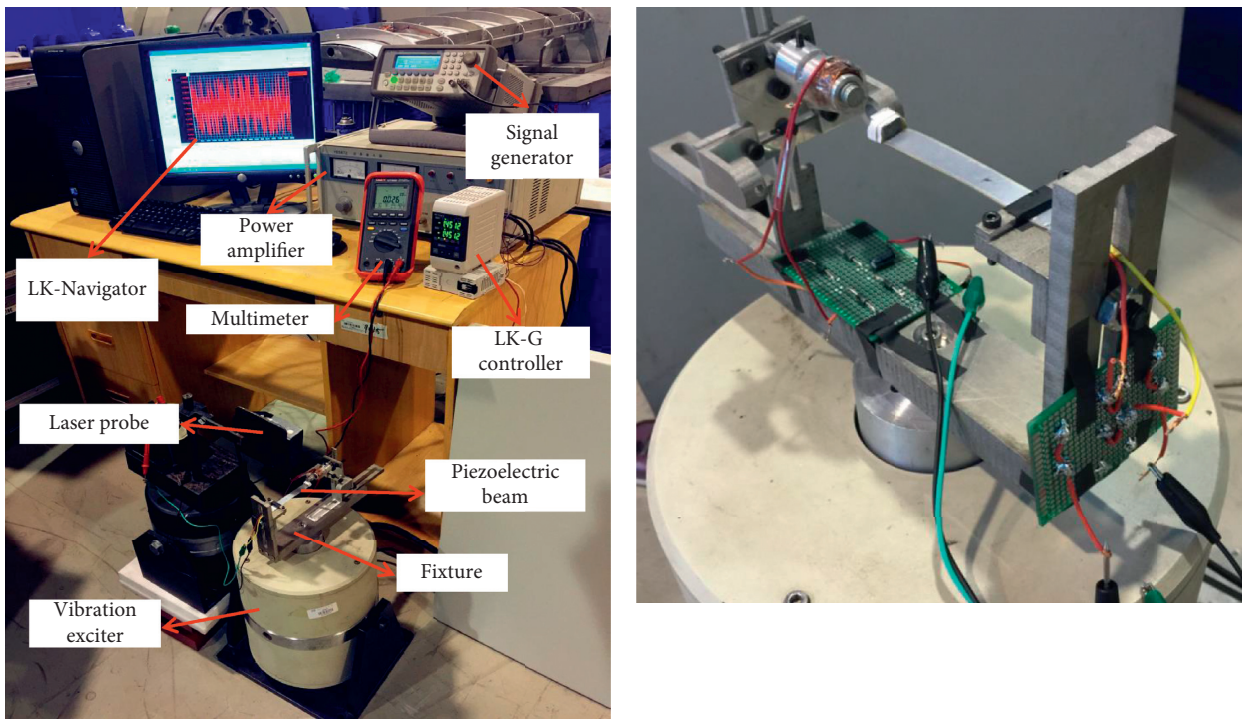

(a) (b)

Figure 1: Experimental setups: (a) experimental apparatus; (b) experimental fixture and circuit.

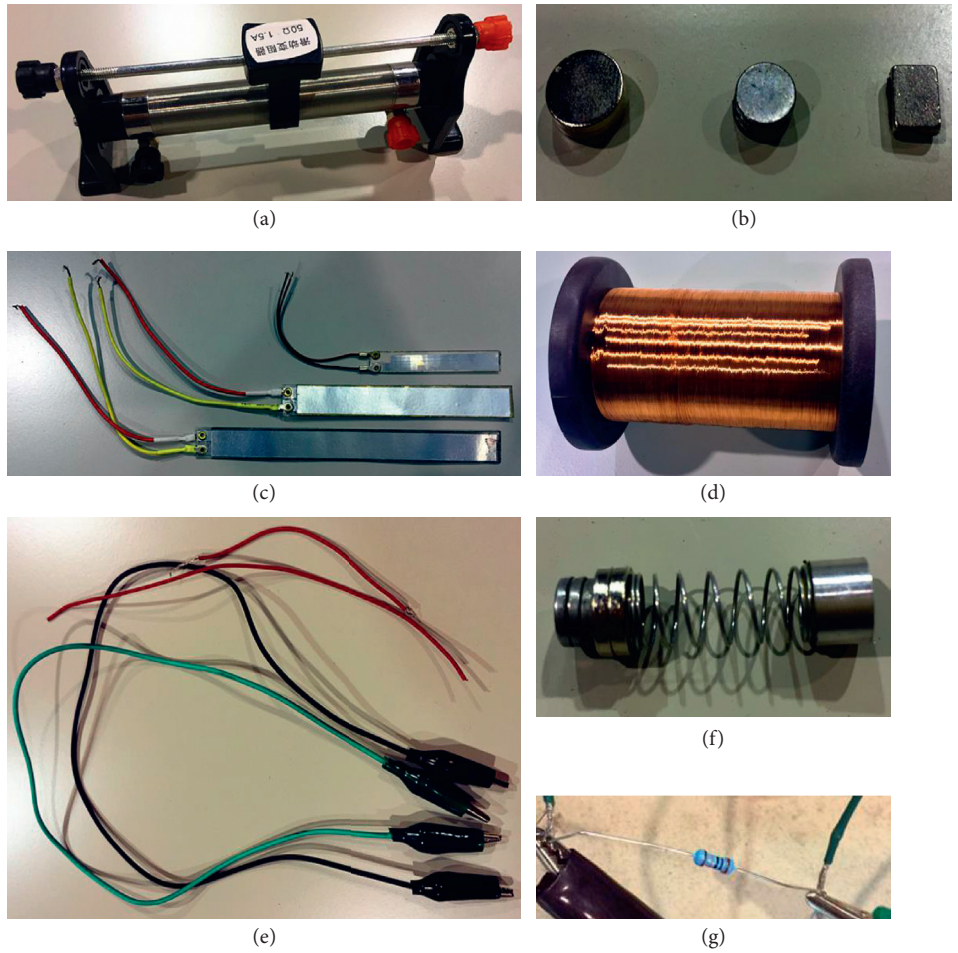

(a) (b)

(c) (d)

(f)

(e) (g)

Figure 2: Experimental materials: (a) variable resistance; (b) magnet; (c) PVDF piezoelectric beam; (d) coil; (e) wire; (f) spring and magnet connection; (g) load.

$G = 8 \times 10^{10}$ Pa; d is the initial wire diameter of the spring and $d = 0.5$ mm; and D represents the initial diameter of the spring and $D = 8.5$ mm. The spring does the telescopic movement with a large amplitude when the magnetic force is weak.

4. Potential Energy of the Bistable Experimental Model

At present, most of scholars have investigated the monostable piezoelectric-electromagnetic combined power generation structure. Since the monostable structure has some disadvantages, a bistable model for the piezoelectric cantilever beam power generation structure is proposed. Moreover, a coil is added to introduce the electromagnetic induction power generation. The model of the structure in this paper is shown in Figure 3. There is a magnet on the opposite position of the piezoelectric cantilever beam, which is fixed at the end of the soft spring in the sleeve. The inner surface of the sleeve is smooth. The magnet does the reciprocating motion in the sleeve. So, the magnetic flux changes continuously through the coil, which results in generating the electromotance.

Since the formation of the bistable structure is mainly caused by the magnetic potential energy of the system, the analysis of the potential energy for the bistable power generation structure needs to be performed. The bistable beam has two stable positions and an unstable position, as shown in Figure 4(a). The potential function of the bistable piezoelectric-electromagnetic combined generator is established as follows:

$$U = U_S + U_M + U_E, \tag{1}$$

where U_S indicates the structural potential energy, U_M is the magnetic potential energy, and U_E denotes the elastic potential energy.

Based on the von Karman nonlinear strain displacement relation, the strain displacement relation of the x direction is given as follows:

$$S = \frac{\partial u_0}{\partial x} + \frac{1}{2}\left(\frac{\partial w_0}{\partial x}\right)^2 - z\frac{\partial^2 w_0}{\partial x^2}. \tag{2}$$

The constitutive equations of the piezoelectric layer are described as follows:

$$\begin{aligned} T &= CS - dE, \\ D &= dS + \varepsilon E, \end{aligned} \tag{3}$$

where T indicates the stress, D is the electric displacement, C denotes the modulus of the elasticity, S represents the strain, d is the piezoelectric constant, E indicates the electric field intensity, and ε denotes the dielectric constant.

Therefore, the structural potential energy of the system is expressed as follows:

$$\begin{aligned} U_S &= \frac{1}{2}\int_v S(CS - dE)\mathrm{d}v - \frac{1}{2}\int_v E(dS - \varepsilon E)\mathrm{d}v, \\ E &= -\frac{V}{(h_3 - h_4)}, \end{aligned} \tag{4}$$

where v is the volume of the piezoelectric beam, V indicates the electric potential difference, and $(h_3 - h_4)$ represents the thickness of piezoelectric layer.

The structural potential energy is obtained as follows:

$$\begin{aligned} U_S = {} & \frac{1}{2}\int_v \left[C\left(\frac{\partial u_0}{\partial x} + \frac{1}{2}\left(\frac{\partial w_0}{\partial x}\right)^2 - z\frac{\partial^2 w_0}{\partial x^2}\right)^2 \right. \\ & \left. + \frac{Vd}{h_3 - h_4}\left(\frac{\partial u_0}{\partial x} + \frac{1}{2}\left(\frac{\partial w_0}{\partial x}\right)^2 - z\frac{\partial^2 w_0}{\partial x^2}\right)\right]\mathrm{d}v \\ & - \frac{1}{2}\int_v \left[-\frac{Vd}{h_3 - h_4}\left(\frac{\partial u_0}{\partial x} + \frac{1}{2}\left(\frac{\partial w_0}{\partial x}\right)^2 \right.\right. \\ & \left.\left. - z\frac{\partial^2 w_0}{\partial x^2}\right) + \frac{\varepsilon V^2}{(h_3 - h_4)^2}\right]\mathrm{d}v. \end{aligned} \tag{5}$$

Next, the magnetic potential energy of the system is established in this section. First of all, the repulsive force of two magnets can be described as follows [38]:

$$\begin{aligned} F_0 = {} & \frac{3}{2(1 + 3d_m)} \times \frac{w_m h_m}{2\mu_k} \times \frac{B_r^2}{\pi^2} \times \left(\tan^{-1}\frac{w_m h_m}{2d_m\sqrt{w_m^2 + h_m^2 + 4d_m^2}} \right. \\ & \left. - \tan^{-1}\frac{w_m h_m}{2d_m(l_m + d_m)\sqrt{w_m^2 + h_m^2 + 4(l_m + d_m)^2}} \right)^2, \end{aligned} \tag{6}$$

where l_m indicates the length of the magnet, w_m is the width of the magnet, h_m denotes the height of the magnet, μ_k represents the magnetic permeability, B_r indicates the magnetic flux density on the magnet polarity surface, and d_m is the distance between two magnets.

The vertical component force F_z of the repulsive force F_0 is related to the displacement w_0 along the vertical direction of the magnet, and it can be written as follows:

$$F_z = F_0 \times \frac{w_0}{\sqrt{w_0^2 + d_m^2}}. \tag{7}$$

The magnetic potential energy is expressed as follows:

$$\begin{aligned} U_M &= \int_0^z F_z \mathrm{d}z \\ &= \frac{k_p}{2d_m}\left(w_0^2 - \frac{1}{4\sqrt{d_m}}\, w_0^4\right), \end{aligned} \tag{8}$$

where k_p represents the repulsive force F_0.

Finally, the elastic potential energy of the system is calculated. The expression for the deformation of the spring is obtained as follows:

$$\Delta x = \frac{F_x}{k_s} = \frac{k_p d_m}{k_s\sqrt{w_0^2 + d_m^2}}, \tag{9}$$

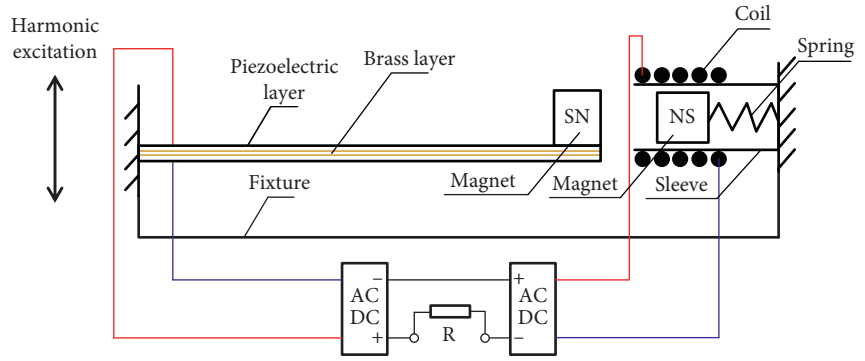

Figure 3: Model of the generator.

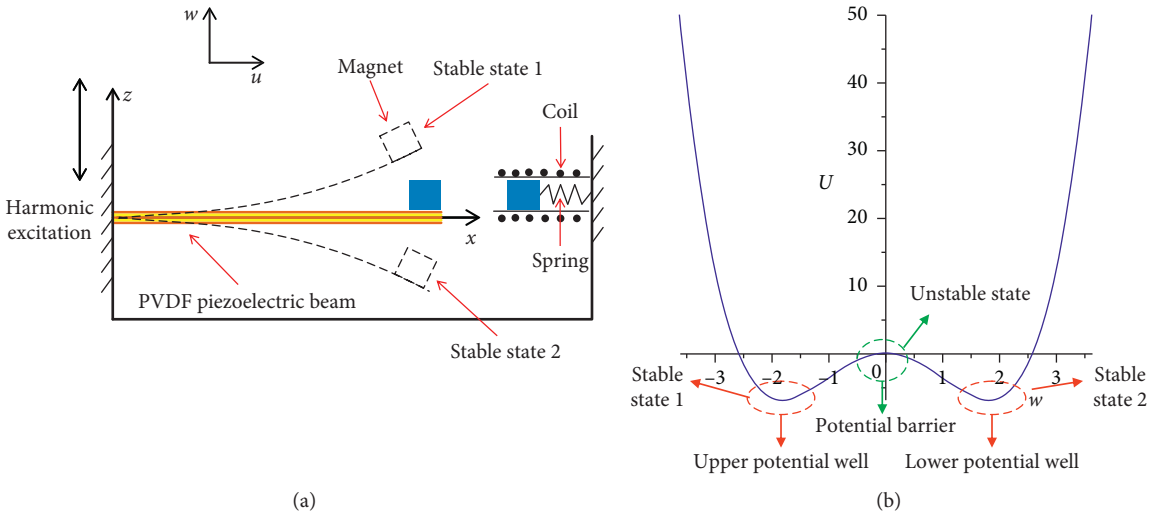

(a) (b)

Figure 4: Bistable model and the potential curve of the structure: (a) mechanical model of the structure; (b) the relation of the potential well and the bistable state.

where k_s indicates the stiffness coefficient of the spring.

The elastic potential energy of the system is written as follows:

$$U_E = \frac{1}{2} k_s \Delta x^2 = \frac{k_p^2 d_m^2}{2k_s\left(w_0^2 + d_m^2\right)}. \tag{10}$$

Substituting equations (5), (8), and (10) into equation (1), the potential function is obtained as follows:

$$\begin{aligned} U = {} & \frac{1}{2}\int_v \left[C\left(\frac{\partial u_0}{\partial x} + \frac{1}{2}\left(\frac{\partial w_0}{\partial x}\right)^2 - z\frac{\partial^2 w_0}{\partial x^2}\right)^2 + \frac{Vd}{h_3 - h_4}\left(\frac{\partial u_0}{\partial x} + \frac{1}{2}\left(\frac{\partial w_0}{\partial x}\right)^2 - z\frac{\partial^2 w_0}{\partial x^2}\right)\right] \mathrm{d}v \\ & - \frac{1}{2}\int_v \left[\frac{Vd}{h_3 - h_4}\left(\frac{\partial u_0}{\partial x} + \frac{1}{2}\left(\frac{\partial w_0}{\partial x}\right)^2 - z\frac{\partial^2 w_0}{\partial x^2}\right) + \frac{\varepsilon V^2}{\left(h_3 - h_4\right)^2}\right] \mathrm{d}v \\ & + \frac{k_p}{2d_m}\left(w_0^2 - \frac{1}{4\sqrt{d_m}} w_0^4\right) + \frac{k_p^2 d_m^2}{2k_s\left(w_0^2 + d_m^2\right)}. \end{aligned} \tag{11}$$

Based on the practical working condition of the structure and theoretical and numerical studies given by Arrieta et al. [9, 10], it is known that vibrations of the first-order mode for the beam play an important role during vibration. The power

generation of the bistable piezoelectric-electromagnetic combined structure mainly depends on vibration of the first-order mode in the beam. Galerkin approach is applied to obtain ordinary differential equations for the potential of the system. Galerkin approach is derived by the Taylor expansion method, which is a mathematically convergent method. Thus, the first-order discretization of equation (11) is expressed as follows:

$$w_0 = \phi_1(x) w_1(t), \tag{12}$$

where $\phi_1(x) = ch\lambda_1 x - \cos\lambda_1 x + ((sh\lambda_1 l - \sin\lambda_1 l)/(ch\lambda_1 l + \cos\lambda_1 l))(sh\lambda_1 x - \sin\lambda_1 x)$.

Substituting equation (12) into equation (11), the potential function is obtained by calculating as follows:

$$U = I_1 w_1^4 - I_2 w_1^3 + I_3 w_1^2 - 2I_4 w_1 + I_5\left(\frac{I_6}{w_1^2 + I_6}\right) - I_7, \tag{13}$$

where $I_0 = (1/l)\int_0^l [\phi_1'(x)]^2 \mathrm{d}x$, $I_1 = (1/2)\int_0^1 \int_v C I_0^2 \phi_1(x) \mathrm{d}v\,\mathrm{d}x - \int_0^1 (k_p/8d\sqrt{d})\phi_1^5(x)\mathrm{d}x$, $I_2 = \int_0^1 \int_v C I_0 \phi_1(x)\phi_1''(x) z \mathrm{d}v\,\mathrm{d}x$, $I_3 = (1/2)\int_0^1 \int_v C\phi_1(x)[\phi_1''(x)]^2 z \mathrm{d}v\,\mathrm{d}x + \int_0^1 \int_v (V\,dI_0/(h_3 - h_4))\phi_1(x)\mathrm{d}v\,\mathrm{d}x + \int_0^1 (k_p/2d_m)[\phi_1(x)]^3 \mathrm{d}x$, $I_4 = (1/2)\int_0^1 \int_v (V\,d/(h_3 - h_4))\phi_1(x)\phi_1''(x) z \mathrm{d}v\,\mathrm{d}x$, $I_5 = (1/2)\int_0^1 (k_p^2/2k_s)\phi_1(x)\mathrm{d}x$, $I_6 = (d_m^2/\phi_1^2(x))$, and $I_7 = (1/2)\int_0^1 \int_v (\varepsilon V^2/(h_3 - h_4)^2)\phi_1(x)\mathrm{d}v\,\mathrm{d}x$.

Bistable states of the system exist in a certain practical physical parameter range. The potential energy equation (13) of the system is derived from the practical bistable model. Since we have conducted a series of experimental studies in this paper, in the process of experiments, we need to compare experimental results by changing the practical parameters, such as magnetic distances, coils, and loads. Thus, parameters of the model are not unique. In order to ensure the universality of the study, dimensionless parameters were used. The parameters of equation (13) are selected as $I_1 = 0.6$, $I_2 = 0.06$, $I_3 = -4$, $I_4 = -0.1$, $I_5 = 0.2$, $I_6 = 0.3$, and $I_7 = 0.1$, and Figure 4(b) is obtained by Maple software. Conclusions can be drawn from Figures 4(a) and 4(b) that the structure has two stable states, which correspond to the upper potential well and the lower potential well. The structure has one unstable state, which corresponds to the potential barrier. Therefore, the generator is the bistable structure. When the piezoelectric cantilever beam obtains the enough large energy to go through the potential barrier, the structure can vibrate between the two stable states. Thus, the frequency bandwidth of the power generation for the structure is broadened. The power generation efficiency of the structure is greatly improved. The schematic diagram of the overall experimental model is shown in Figure 5.

The power generation structure with the bistable states and multimode generates much larger energy when the beam produces a large amplitude vibration. Since the spring is soft, the magnet moves fast inside the coil when the piezoelectric beam vibrates between two stable positions. When the piezoelectric cantilever beam moves from each stable position to the unstable position, the repulsive force between magnets increases gradually. Based on the bistable structure, the spring component is introduced. When the spring is compressed, the repulsive force of the structure with the spring is smaller than that of the structure without the spring. Under the case of the spring, the energy required to pass through the barrier is reduced in the structure. The piezoelectric cantilever beam is easier to go through the potential barrier. The combination of the bistable states and multimode structure makes the piezoelectric beam vibrate between two stable positions easily, and the power generation efficiency of the system is greatly improved. Therefore, the piezoelectric-electromagnetic combined generator has much a greater power generation efficiency.

5. Experimental Result Analysis

The power generation efficiency and dynamic behaviors of the piezoelectric-electromagnetic combined generator are investigated. The power generation efficiency of the single piezoelectric cantilever beam structure and the piezoelectric-electromagnetic combined power generation structure is compared. Then, magnetic distances, coils, and loads of the structure are optimized. The diagrams of experimental setups are shown in Figure 6. Figures 6(a) and 6(b) indicate the piezoelectric cantilever beam placed in the upper potential well and the lower potential well, respectively. In the experiment, three different kinds of power generation structures are studied, as shown in Figure 7. The structure A is the conventional monostable piezoelectric cantilever beam structure. The structure B indicates the bistable piezoelectric cantilever beam structure introduced the spring and the magnet. The structure C is the bistable piezoelectric-electromagnetic combined power generation structure, which introduced the spring, the magnet, and the coil.

5.1. Power Generation Efficiency of Structures

5.1.1. Influence of Excitation Frequencies on the Power Generation of Structures. Firstly, the power generation of the structure A and the structure B is investigated. In order to ensure the reliability of the experimental results, four groups of experiments are performed under the conditions of different magnetic distances. The external excitation is given in the form of the sinusoidal signal $A\sin\omega t$. The external excitation amplitude is selected as 2.5 V. The external excitation frequency increases from 5 Hz to 20 Hz with 0.2 Hz step size. In the experiment, the effective output voltage is defined to compare the effective frequency bandwidth of different structures. Thus, it is assumed that the effective output voltage is greater than or equal to 3 V. The effective frequency bandwidth is the difference between the maximum external excitation frequency and the minimum external excitation frequency in the range of the effective voltage. In the experiment, the maximum output voltage of the structure A is 12.337 V, and the effective frequency bandwidth of structure A is 4 Hz.

In the first group, the magnetic distance of structure B is 15 mm. The experimental results are shown in Figure 8, in

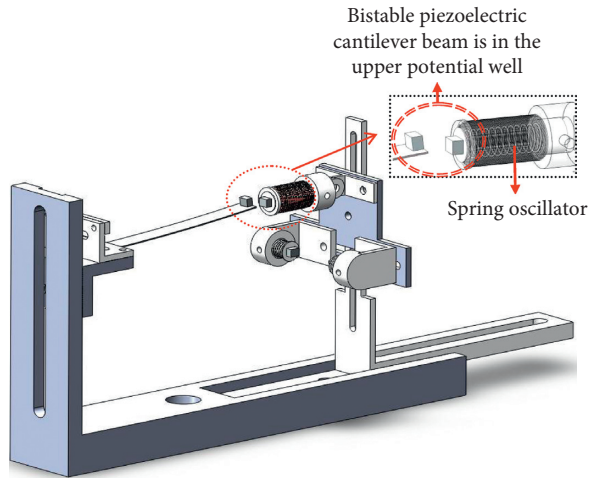

Figure 5: Schematic diagram of the experimental model.

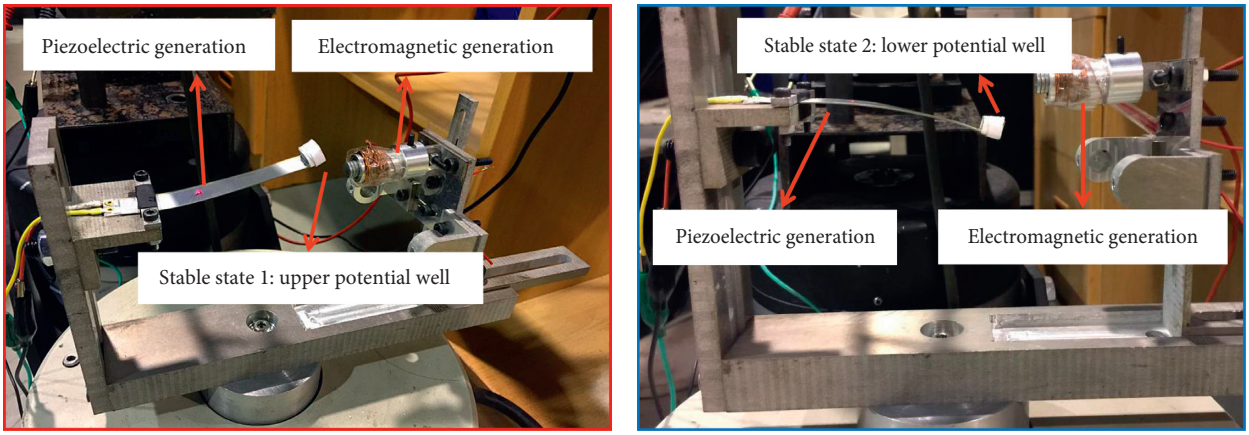

(a) (b)

Figure 6: Diagrams of experimental setups: (a) structure is placed in the upper potential well; (b) structure is placed in the lower potential well.

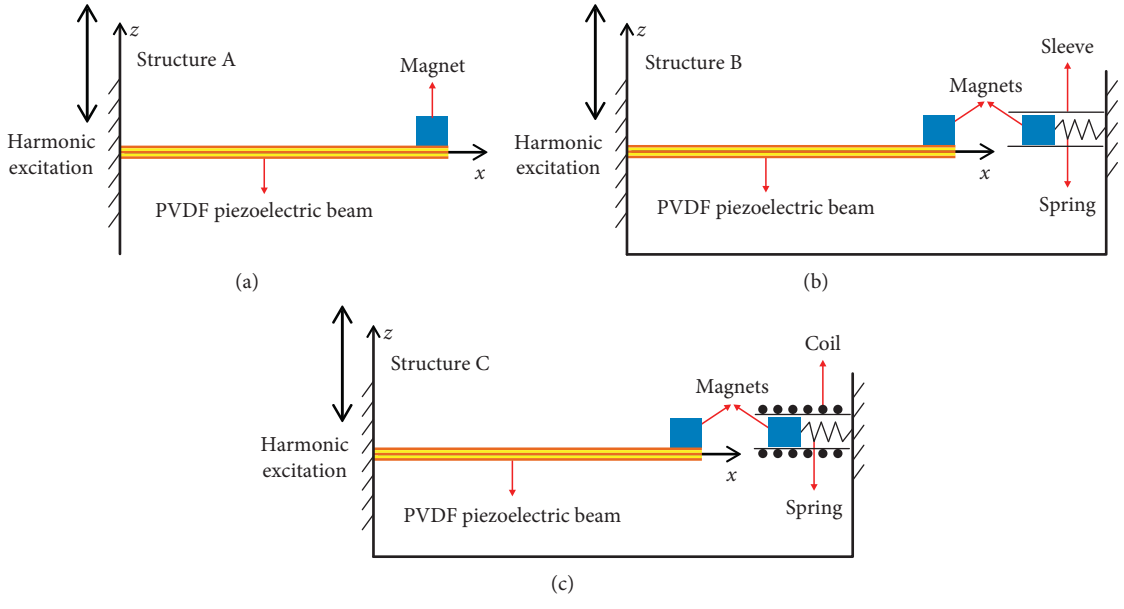

Figure 7: Three kinds of structures: (a) structure A; (b) structure B; (c) structure C.

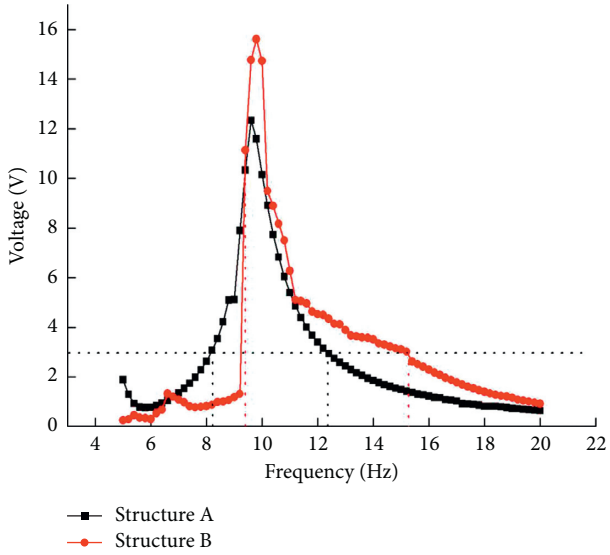

Figure 8: Relation of the frequency-voltage of the structure A and the structure B is given when the initial magnetic distance of the structure B is 15 mm.

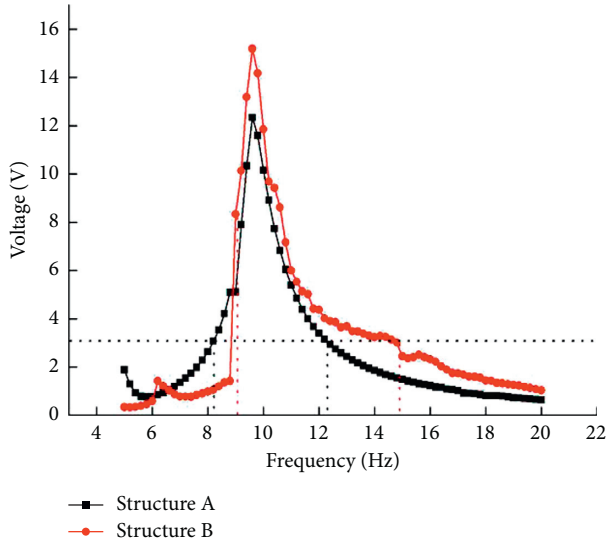

Figure 9: Relation of the frequency-voltage of the structure A and the structure B is given when the initial magnetic distance of the structure B is 14 mm.

which the maximum output voltage of structure B is 15.214 V. The output voltage of structure B is greater than that of structure A. The range of two black dashed lines, which are vertical to the horizontal axis, is the effective frequency bandwidth of structure A, as shown in Figure 8. The range of two red dashed lines is the effective frequency bandwidth of structure B, as shown in Figure 8. The effective frequency bandwidth of structure B is 5.8 Hz. The effective frequency bandwidth of structure B is wider than that of structure A.

In the second group, the magnetic distance of structure B is 14 mm. The results can be seen from Figure 9 that the maximum output voltage of structure B is 14.882 V. The maximum output voltage of the bistable structure B is greater than that of the monostable structure A. The effective frequency bandwidth of structure B is 5.8 Hz. Comparing with structure A, the effective frequency bandwidth of structure B is broadened.

In the third group, the magnetic distance of structure B is 13 mm. It can be shown from Figure 10 that the maximum output voltage of structure B is 12.478 V. The maximum output voltage of the system is improved. The effective frequency bandwidth of structure B is 6.2 Hz. The effective frequency bandwidth of the system is broadened.

In the fourth group, the magnetic distance of structure B is 12 mm. The effective frequency bandwidth of the system is 4 Hz. Since the magnetic distance of 12 mm is too small, the repulsive force between two magnets is too great. The piezoelectric cantilever beam cannot go through the potential barrier so that the beam cannot conduct a large amplitude vibration. The results show that the magnetic distance is too small to generate the large output voltage.

Based on the above experiments, it is found that the piezoelectric cantilever beam is easier to go through the potential barrier when the spring and the magnet are introduced under the condition of a suitable magnetic

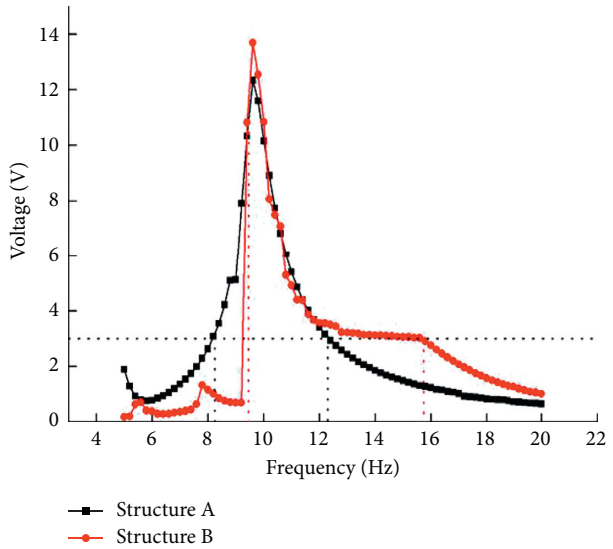

Figure 10: Relation of the frequency-voltage of the structure A and the structure B is given when the initial magnetic distance of the structure B is 13 mm.

distances. Therefore, the cantilever beam produces large amplitude vibrations in a wide range of frequencies. The effective frequency bandwidth of the system is broadened under the case of a suitable magnetic distance after the spring is introduced.

In the following experiment, the power generation of structure B and structure C is studied. Experiments are carried out to confirm what the range of magnetic distances is good for the power generation of structure B and structure C. It is found that the power generation efficiency of the system is relatively great when the magnetic distance is from 11 mm to 16 mm. Therefore, the magnetic distances of this experiment are 11 mm, 12 mm, 13 mm, 14 mm, 15 mm, and

16 mm. The comparison of the power generation efficiency of structure B and structure C under the different magnetic distances is given, as shown in Table 1. Based on the bistable piezoelectric cantilever beam structure with the spring and the magnet, it is found that the output voltage is improved, and the effective frequency bandwidth is broadened when the coil is introduced. According to Table 1, the maximum output voltage of structure B and structure C is further compared, as shown in Figure 11. It can be seen in Figure 11 that the introduction of the coil improves the maximum output voltage of structure C. The conclusion is drawn that the power generation efficiency of structure C is the best among three kinds of structures.

Subsequently, the influence of excitation frequencies on the power generation of structure C under the different magnetic distances is studied. Figure 12 is obtained when magnetic distances are 12 mm, 13 mm, 14 mm, and 15 mm, respectively. It can be observed from Figure 12 that the output voltage of the system is quite small when the structure just starts to vibrate in the low-frequency range. When the external excitation frequency increases to 9.5 Hz, the piezoelectric cantilever beam goes through the potential barrier to perform a larger amplitude vibration. The output voltage of the system improves sharply. The structure generates the maximum output voltage when the external excitation frequency is about 9.8 Hz. When the external excitation frequency continues to increase, the output voltage decreases gradually. Therefore, the power generation efficiency of the structure is the best when the external excitation frequency is near the frequency of passing through the potential barrier.

It is found from Figure 12 that the power generation efficiency of the structure is very small when the magnetic distance is 12 mm. Since the magnetic distance is less than 12 mm, the magnetic force is too great. The energy required becomes greatly when the cantilever beam goes through the potential barrier. So, the cantilever beam cannot go through the potential barrier easily. The cantilever beam only conducts small amplitude vibration near the one stable position, and the power generation efficiency of the system is not good. The conclusion can be obtained that the power generation efficiency of structure C can be improved under suitable magnetic distances.

5.1.2. Influence of External Excitation Amplitudes on the Power Generation of Structures. In the above experiment, the piezoelectric cantilever beam goes through the potential barrier when the external excitation frequency is about 9.5 Hz. So, the external excitation frequency is selected as 9.5 Hz. The external excitation amplitude increases from 0.5 V to 2.5 V with 0.1 V step size. The magnetic distances are 13 mm, 14 mm, and 15 mm, respectively. The experimental results are shown in Table 2. Compared with the output voltage of structure B, the output voltage of structure C improves 6.2% when the magnetic distance is 15 mm. The output voltage of structure C is improved 8.29% than that of structure B when the magnetic distance is 14 mm. Compared with structure B, the output voltage of structure C improves 1.72% when the magnetic distance is 13 mm.

In this section, we mainly discuss the influence of external excitation amplitudes on the power generation of three different kinds of structures. Conclusions are obtained from Figure 13 that the power generation efficiency of structure B and structure C is worse than that of structure A when the external amplitude is less than 1.3 V. Since the cantilever beam cannot go through the potential barrier, the structures show the monostable vibration behaviors and the power generation efficiency of the structures are quite small. When the cantilever beam goes through the potential barrier, the output voltage of structure B and structure C improves greatly. The output voltages of structure B and structure C are greater than that of structure A. It is found from Figure 13 that the output voltage of structure B and structure C improves rapidly when the external excitation amplitude is greater than 2.3 V.

5.2. Dynamic Behaviors of Structures. The power generation efficiency of structures mainly depends on two factors, which one is the output frequency bandwidth and the other is the output voltage of the structure. In the above experimental studies, we mainly analyze the influence of external excitation frequencies and amplitudes on the power generation of structures in order to determine what structure produces the most largest power generation. Based on the experimental results, we have drawn the following conclusions:

(1) From the opinion of the output frequency bandwidth, the power generation of structure B is better than that of structure A, and the power generation of structure C is better than that of structure B. The output frequency bandwidth of structure C is the best among three kinds of structures.

(2) From the opinion of the output voltage, the output voltages of structure B and structure C are greater than that of structure A when the external excitation amplitude is greater than 2.3 V. Structure B and structure C produce almost the same amount of the output voltage.

(3) In a word, the power generation efficiency of the structure C is the best among three kinds of structures, and the power generation of the structure A is the worst. Structure A is the monostable structure, and both structure B and structure C are bistable structures. Since the output frequency bandwidth of the bistable structure is wider than that of the monostable structure, the power generation efficiency of structures B and C is better than that of structure A.

(4) The power generation capacity of the bistable structure depends on the nonlinear dynamic characteristics of the structure. So, complicated dynamical behaviors of structures A and C need to be further analyzed. In order to find the advantages of dynamical characteristics for the bistable structure, dynamic behaviors of the monostable structure and the bistable structure are comparatively studied.

Table 1: Comparison of the power generation efficiency of the structure A, the structure B, and the structure C is given when the external excitation frequency is studied.

Magnetic distance (mm)	Structure	Freq (Hz)	V (V)	V%	$\overline{V}$%
—	A	4	12.337	—	—
16	B	4.4	10.127	13.8	9.14
	C	5.4	11.521		
15	B	5.8	15.214	6.71	10.11
	C	6.8	15.806		
14	B	5.8	14.882	3.47	7.81
	C	7.2	15.399		
13	B	6.2	12.478	10.44	19.24
	C	7.0	13.781		
12	B	4	6.634	7.21	4.14
	C	4.2	7.112		
11	B	1.6	4.26	13.8	8.21
	C	1.8	4.85		

A is the conventional monostable piezoelectric cantilever beam; B indicates the bistable piezoelectric cantilever beam with the spring and the magnet; C indicates the bistable piezoelectric cantilever beam with the spring, the magnet, and the coil. Freq indicates the effective frequency bandwidth of structures; V indicates the maximum output voltage; V% indicates the growth rate of the maximum output voltage; $\overline{V}$% indicates the average growth rate of the output voltage.

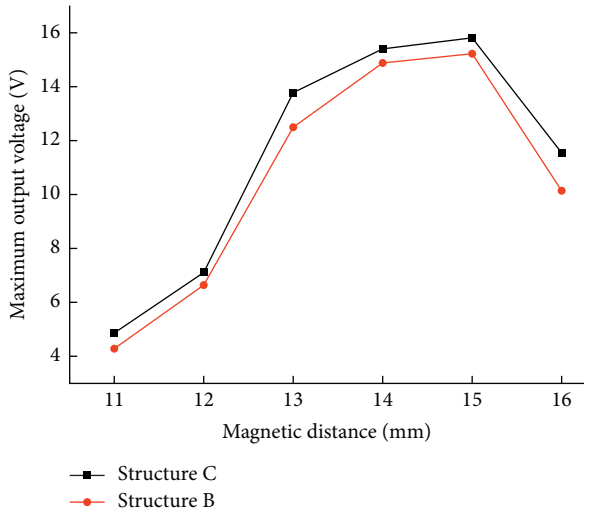

Figure 11: Maximum output voltage of the structure B and the structure C.

According to the above experiment of the influence of external excitation amplitudes on the power generation of structures, it is found that the output voltage of structure C improves rapidly when the external excitation amplitude is greater than 2.3 V. But, the maximum excitation amplitude, which the experimental equipment can provide, is 2.5 V. Thus, the external excitation amplitude is selected as 2.5 V in this experiment. In the previous experiment, the power generation efficiency of the structures is worse when the excitation frequency is greater than 30 Hz. Therefore, the external excitation frequency increases from 5 Hz to 30 Hz. Dynamic behaviors of the piezoelectric cantilever beam are analyzed when magnetic distances are 13 mm, 14 mm, and 15 mm, respectively. Based on the above experiment, we find that the output voltage becomes larger with the increase in the vibration amplitude of the piezoelectric beam. The value of the output voltage relies on the amplitude of vibration for the structure.

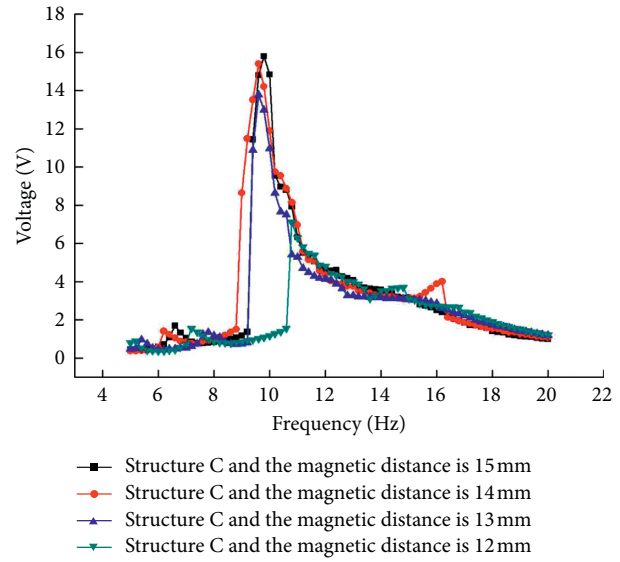

Figure 12: Relation of the voltage-frequency of different magnetic distances.

Table 2: Comparison of the power generation efficiency of the structure A, the structure B, and the structure C is given when the external excitation amplitude is studied.

Magnetic distance (mm)	Structure	V (V)	$\overline{V}$%
—	A	12.281	—
15	B	15.096	6.2
	C	15.246	
14	B	15.065	8.29
	C	15.217	
13	B	13.426	1.72
	C	13.451	

A is the conventional monostable piezoelectric cantilever beam; B indicates the bistable piezoelectric cantilever beam with the spring and the magnet; C indicates the bistable piezoelectric cantilever beam with the spring, the magnet, and the coil. V indicates the maximum output voltage; $\overline{V}$% indicates the average growth rate of the output voltage.

5.2.1. Dynamic Behaviors of the Structure A. When the external excitation frequency is changed from 5 Hz to 20.6 Hz, dynamic behaviors of the cantilever beam show the period-1 motion, as shown in Figure 14. When the external excitation frequency is changed from 20.6 Hz to 30 Hz, dynamic behaviors of the quasiperiod motion are obtained, as shown in Figure 15. In the experimental study of this paper, the material of the piezoelectric cantilever beam is PVDF, which is relatively flexible and prone to the large deformation. At the same time, the length-width ratio of the piezoelectric cantilever beam is larger, which is easy to produce the large deformation. Although structure A is a

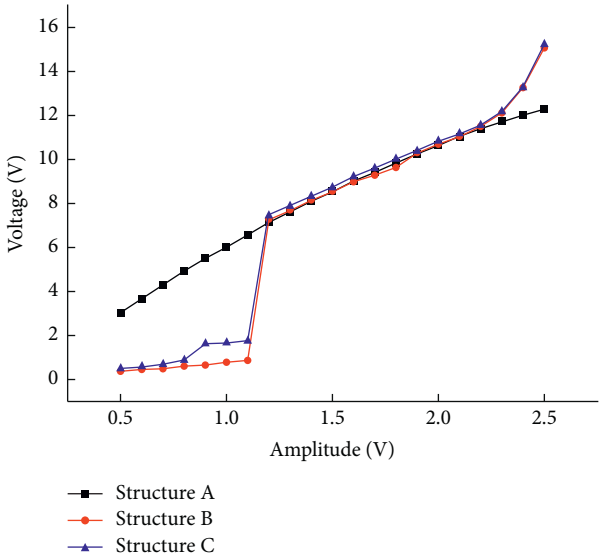

Figure 13: Relation of the voltage-amplitude of three structures is given when magnetic distances of the structure B and the structure C are both 14 mm.

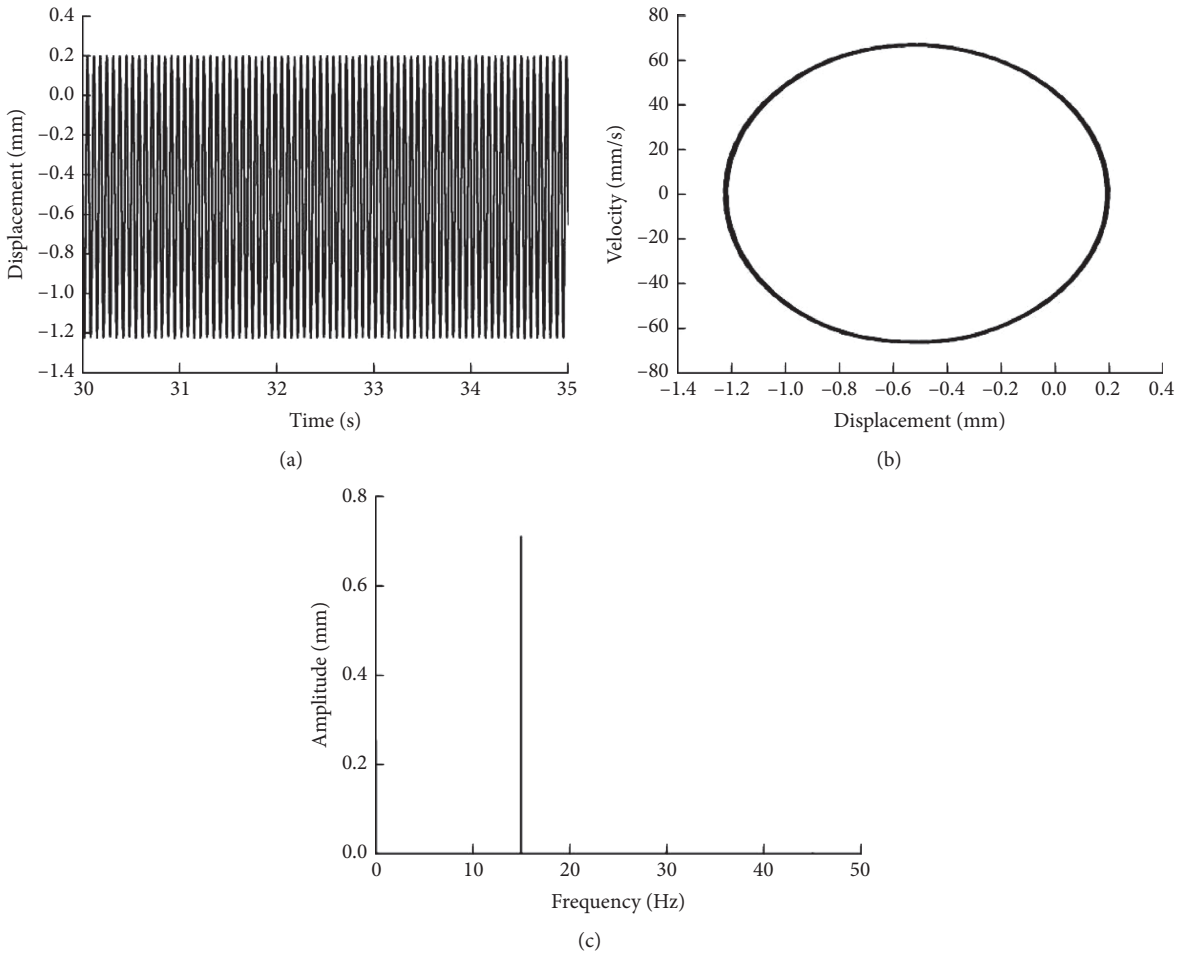

Figure 14: Period-1 motion of the structure A is obtained for the external excitation amplitude $W = 2.5$ V and the external excitation frequency $\Omega = 15$ Hz: (a) waveform; (b) phase portrait; (c) amplitude spectrum.

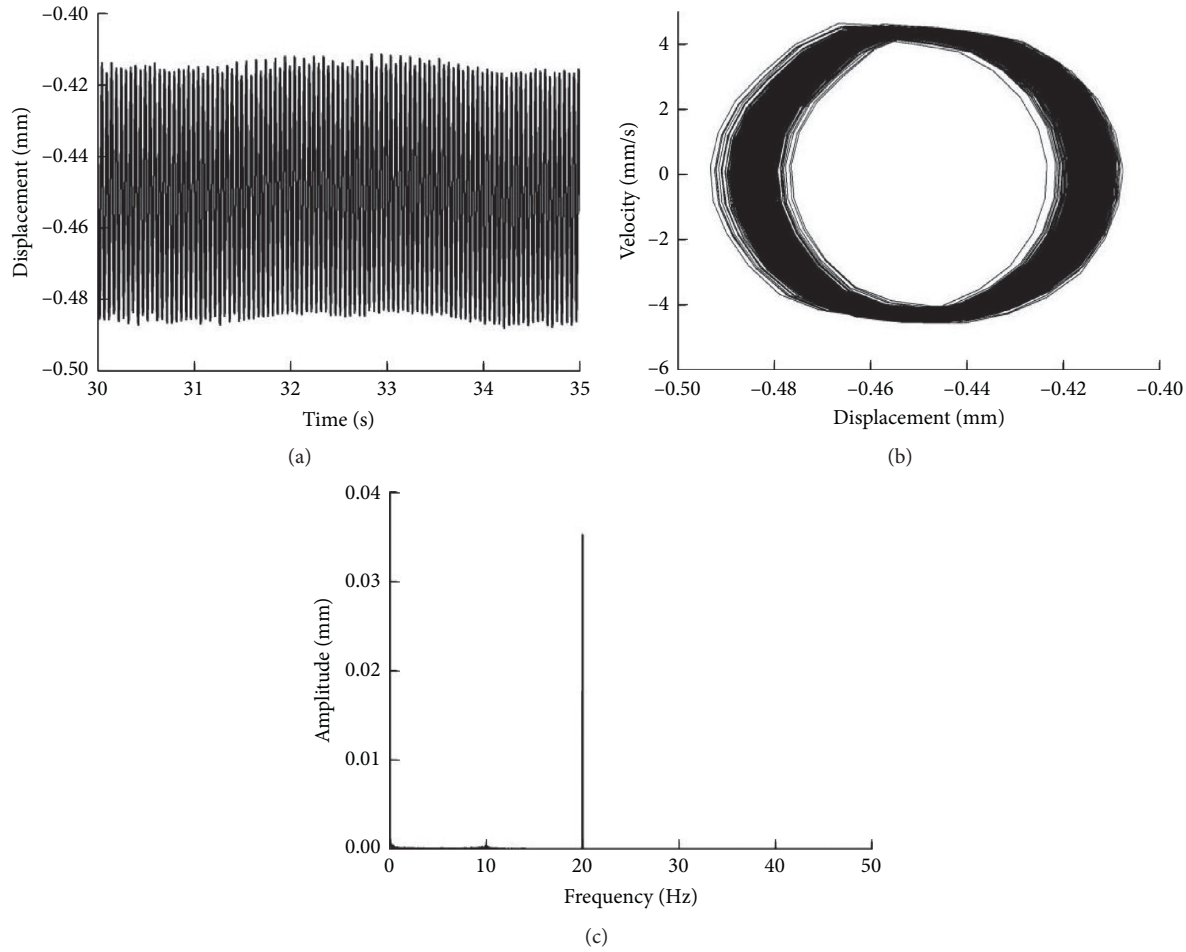

Figure 15: Quasiperiodic motion of the structure A is obtained for the external excitation frequency $\Omega = 20.8$ Hz: (a) waveform; (b) phase portrait; (c) amplitude spectrum.

conventional monostable system, it has nonlinear phenomena. Thus, the quasiperiod motion in structure A is caused by geometric nonlinearity with the large deformation. Dynamic behaviors of structure A are given as follows: period-1 motion $\longrightarrow$ quasiperiod motion. It can be seen from experimental results that nonlinear dynamic behaviors of the conventional monostable piezoelectric cantilever beam are not obvious. The vibration amplitude of the quasiperiod motion for structure A is smaller than that of the period-1 motion. Therefore, the power generation efficiency of the period-1 motion for structure A is better than that of the quasiperiod motion.

5.2.2. Dynamic Behaviors of the Structure C. Dynamic behaviors of structure C are analyzed in this section. When the magnetic distance is chosen as 15 mm, dynamic behaviors of the system change 10 times. When the magnetic distance is selected as 14 mm, dynamic behaviors of the system change 12 times. When the magnetic distance is 13 mm, dynamic behaviors of the system change 10 times. The chaotic motion occurs in vibration of the structure under the conditions of three different magnetic distances. It is observed that rich and complex nonlinear dynamic behaviors occur in vibration of the system when the spring and the magnet are introduced.

Dynamic behaviors of structure C are shown in Figures 16–27 when the magnetic distance is selected as 14 mm. In these figures, (a) is the waveform diagram of the system, (b) is the phase portrait of the system, and (c) is the amplitude spectrum of the system. When the external excitation frequency is from 5 Hz to 10.4 Hz, the period-1 motion appears in the system, as shown in Figure 16. When the external excitation frequency is less than 9.5 Hz, the cantilever beam vibrates only in the upper potential well so that the vibration amplitude of the beam is small and increases slowly. When the external excitation frequency increases to 9.8 Hz, the piezoelectric cantilever beam goes through the potential barrier, and the vibration amplitude of the beam increases sharply. A snap-through phenomenon occurs in the output voltage of the system, in which the output voltage of the system reaches the maximum value. Existence of a snap-through phenomenon corresponds to the period-1 motion in vibration of the system.

When the external excitation frequency increases to 10.4 Hz, Figure 17 shows the occurrence of the chaotic

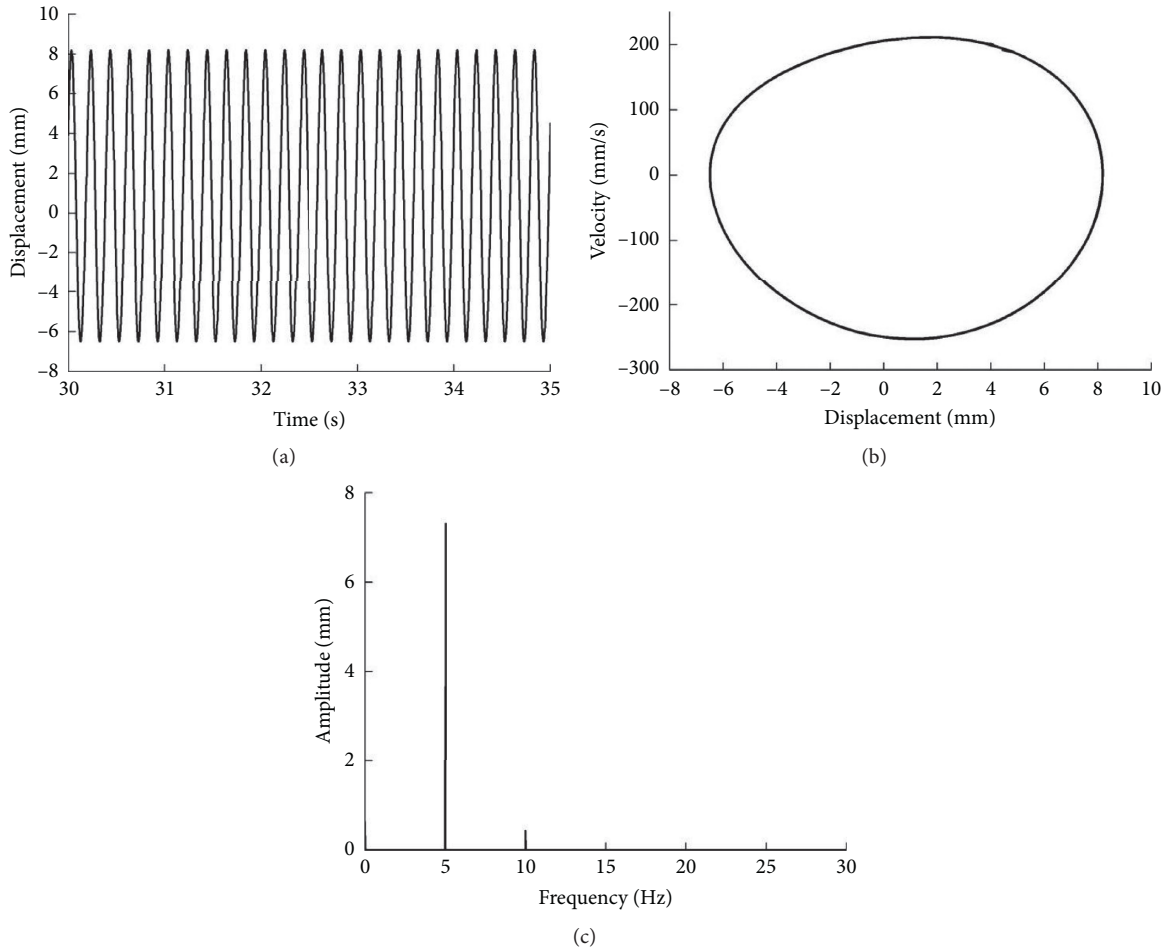

Figure 16: Period-1 motion of the structure C is obtained for the external excitation amplitude $W = 2.5$ V, the external excitation frequency $\Omega = 5$ Hz, and the magnetic distance 14 mm: (a) waveform; (b) phase portrait; (c) amplitude spectrum.

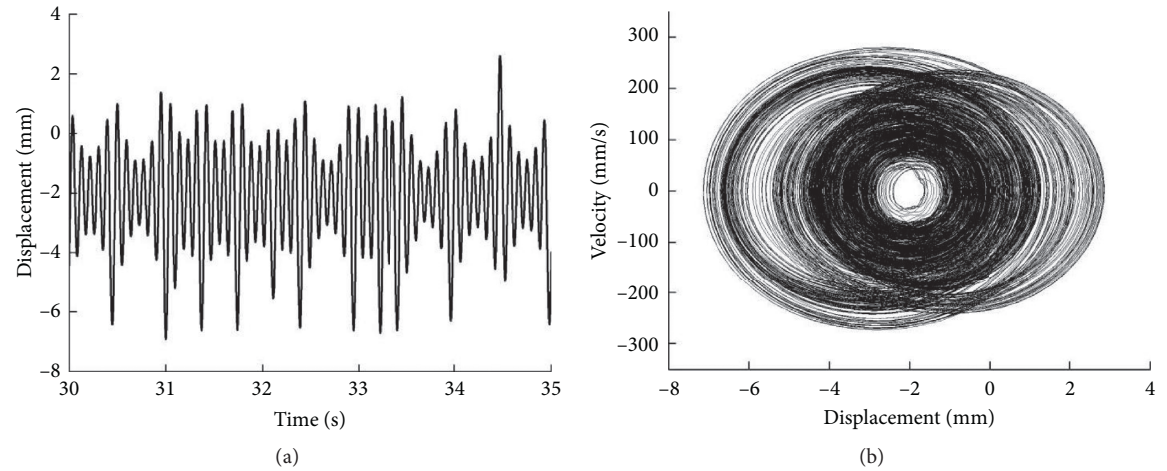

Figure 17: Continued.

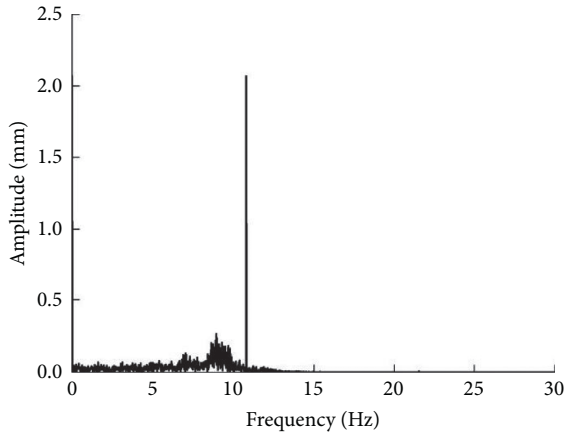

(c)

Figure 17: Chaotic motion of the system is obtained for the external excitation frequency $\Omega = 10.8$ Hz: (a) waveform; (b) phase portrait; (c) amplitude spectrum.

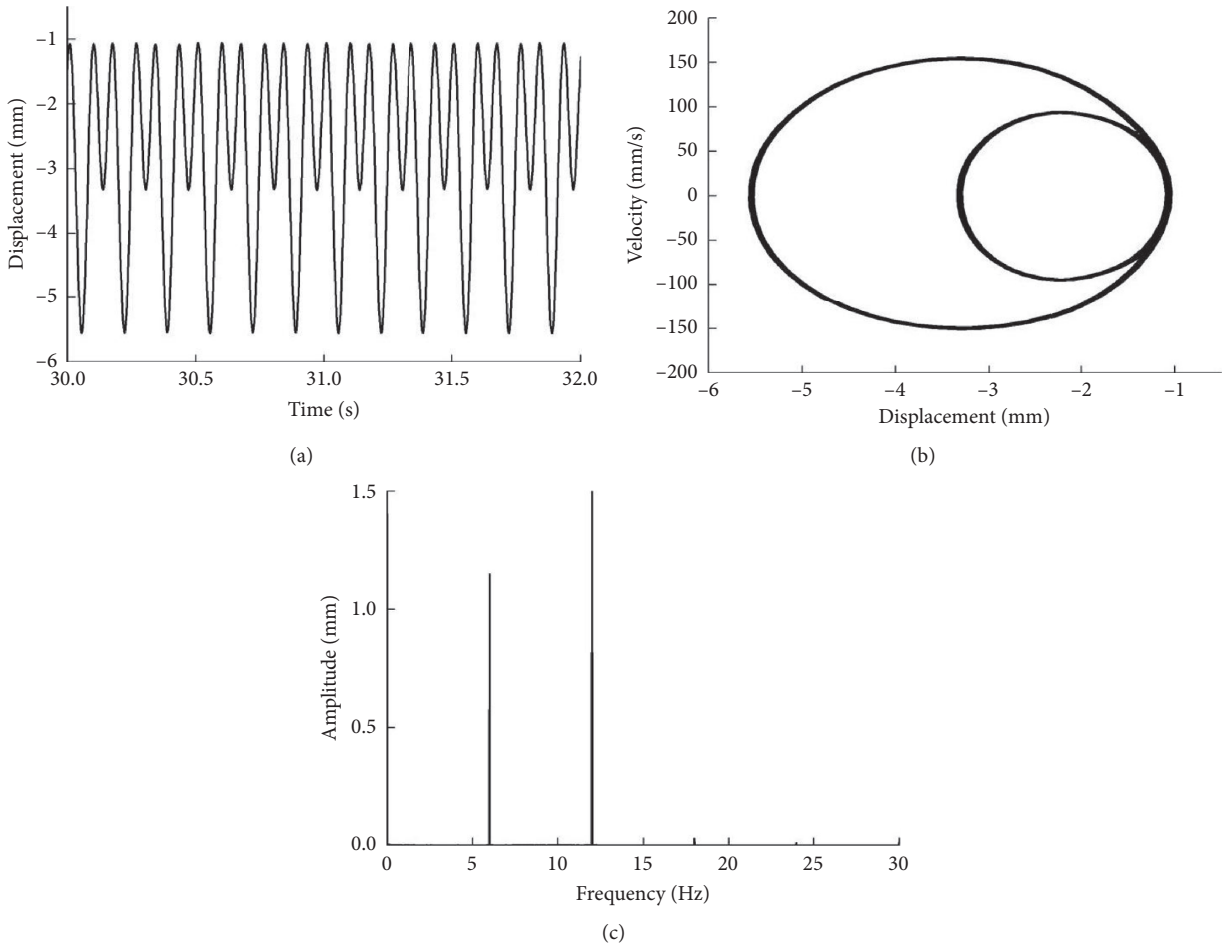

(a)

(b)

(c)

Figure 18: Period-2 motion of the system is obtained for the external excitation frequency $\Omega = 12$ Hz: (a) waveform; (b) phase portrait; (c) amplitude spectrum.

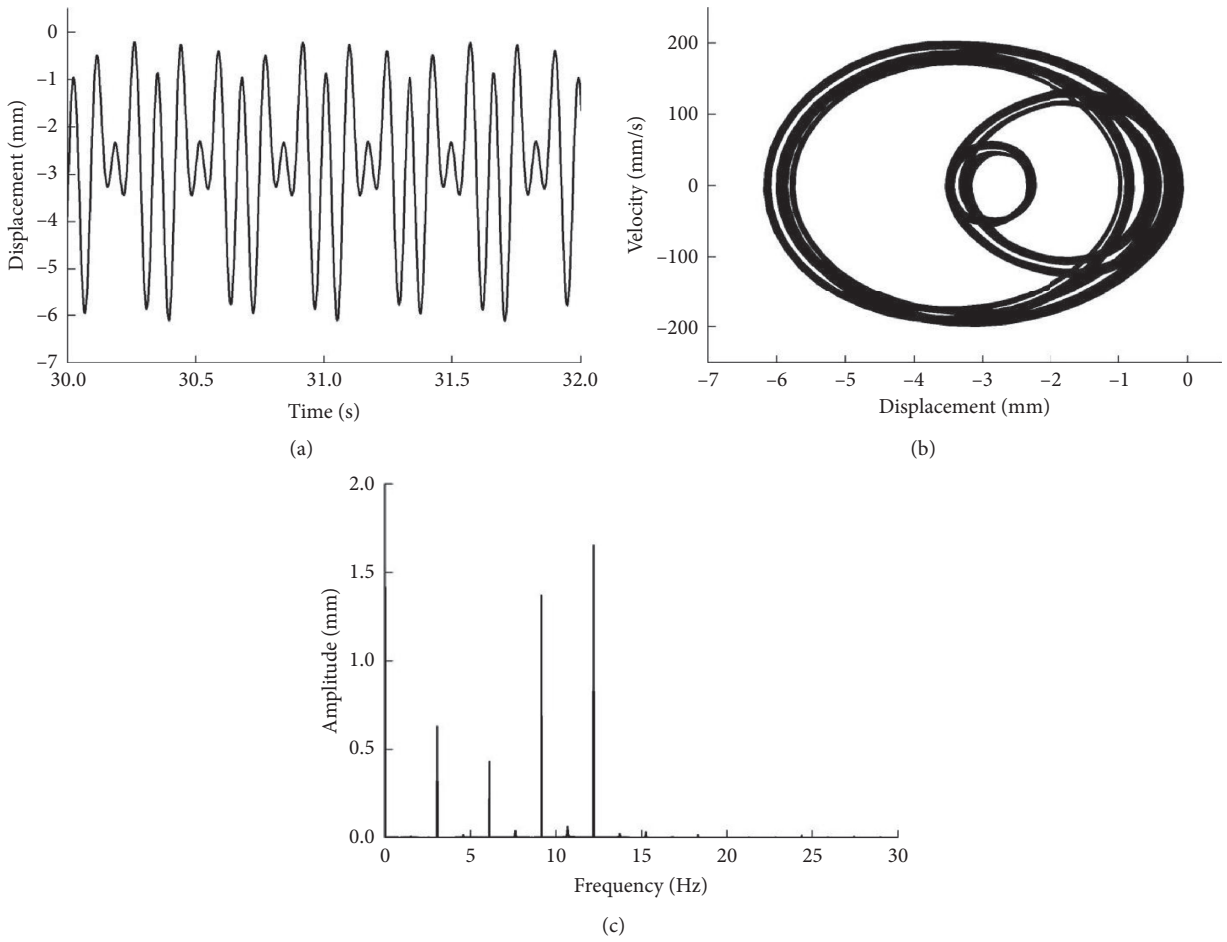

Figure 19: Multiperiod motion of the system is obtained for the external excitation frequency $\Omega = 12.2$ Hz: (a) waveform; (b) phase portrait; (c) amplitude spectrum.

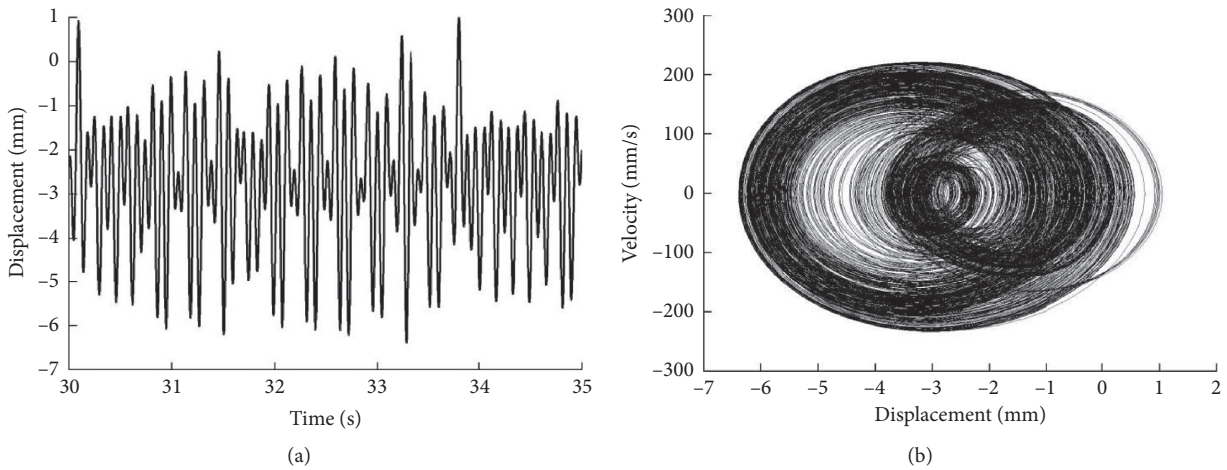

Figure 20: Continued.

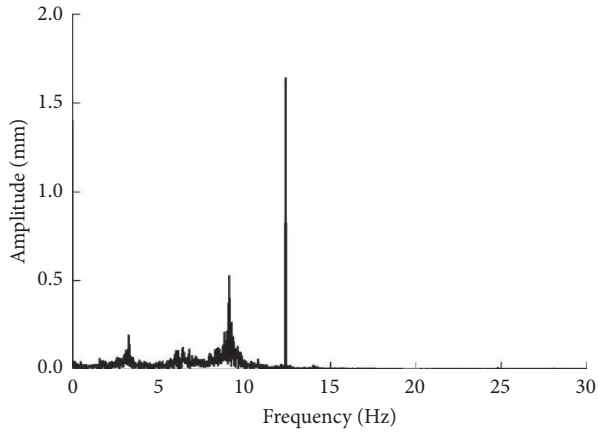

(c)

Figure 20: Chaotic motion of the system is obtained for the external excitation frequency $\Omega = 12.4$ Hz: (a) waveform; (b) phase portrait; (c) amplitude spectrum.

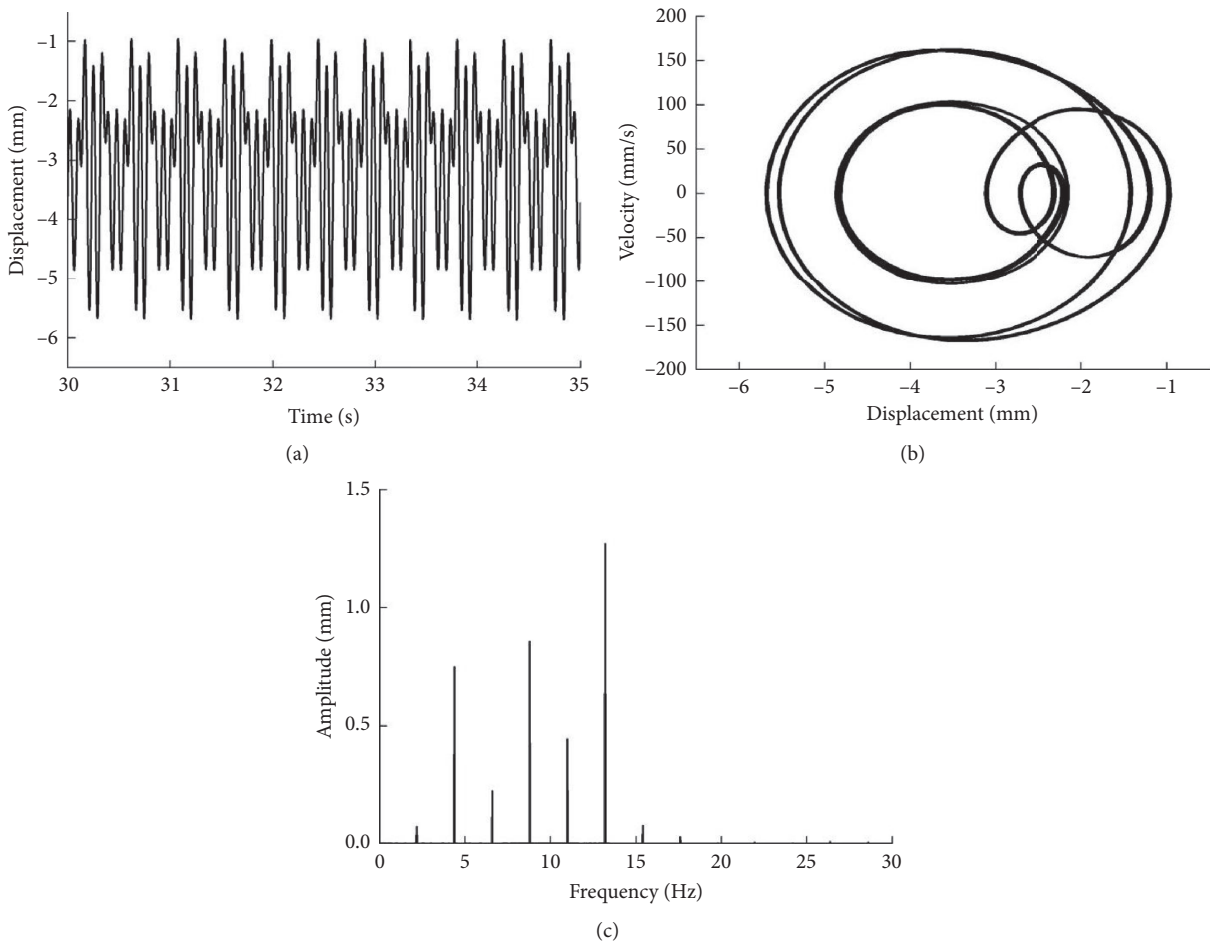

(a)

(b)

(c)

Figure 21: Multiperiod motion of the system is obtained for the external excitation frequency $\Omega = 13.2$ Hz: (a) waveform; (b) phase portrait; (c) amplitude spectrum.

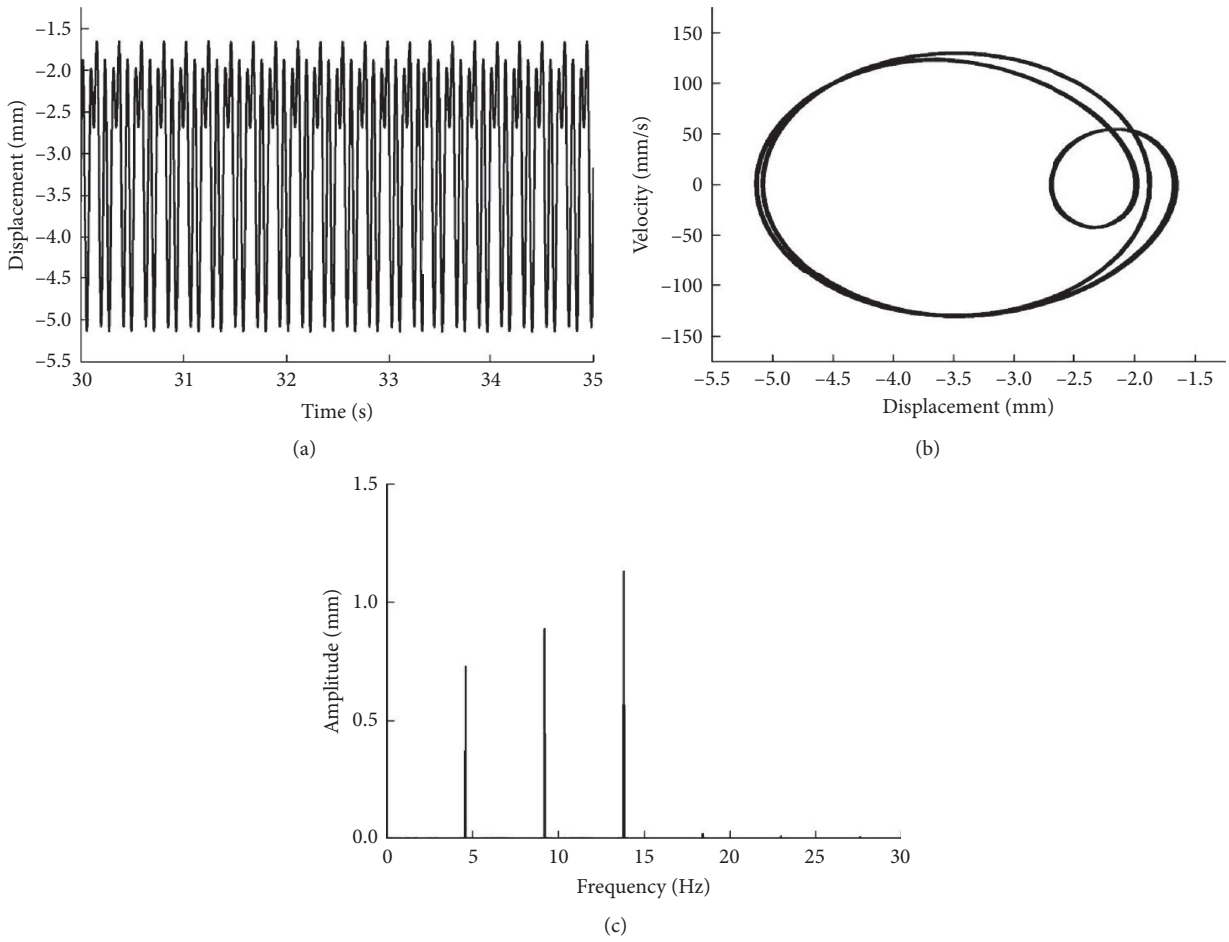

Figure 22: Period-3 motion of the system is obtained for the external excitation frequency $\Omega = 13.8$ Hz: (a) waveform; (b) phase portrait; (c) amplitude spectrum.

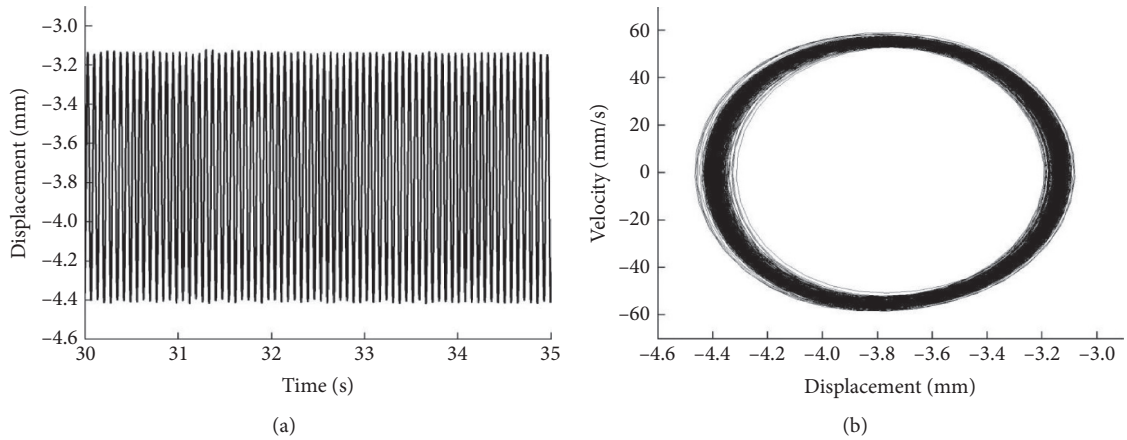

Figure 23: Continued.

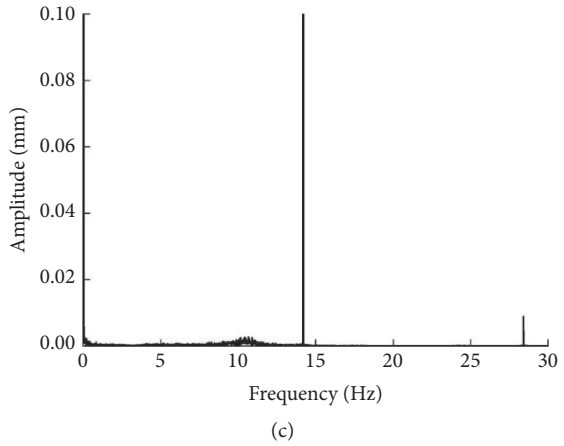

(c)

Figure 23: Quasiperiod motion of the system is obtained for the external excitation frequency $\Omega = 14.2$ Hz: (a) waveform; (b) phase portrait; (c) amplitude spectrum.

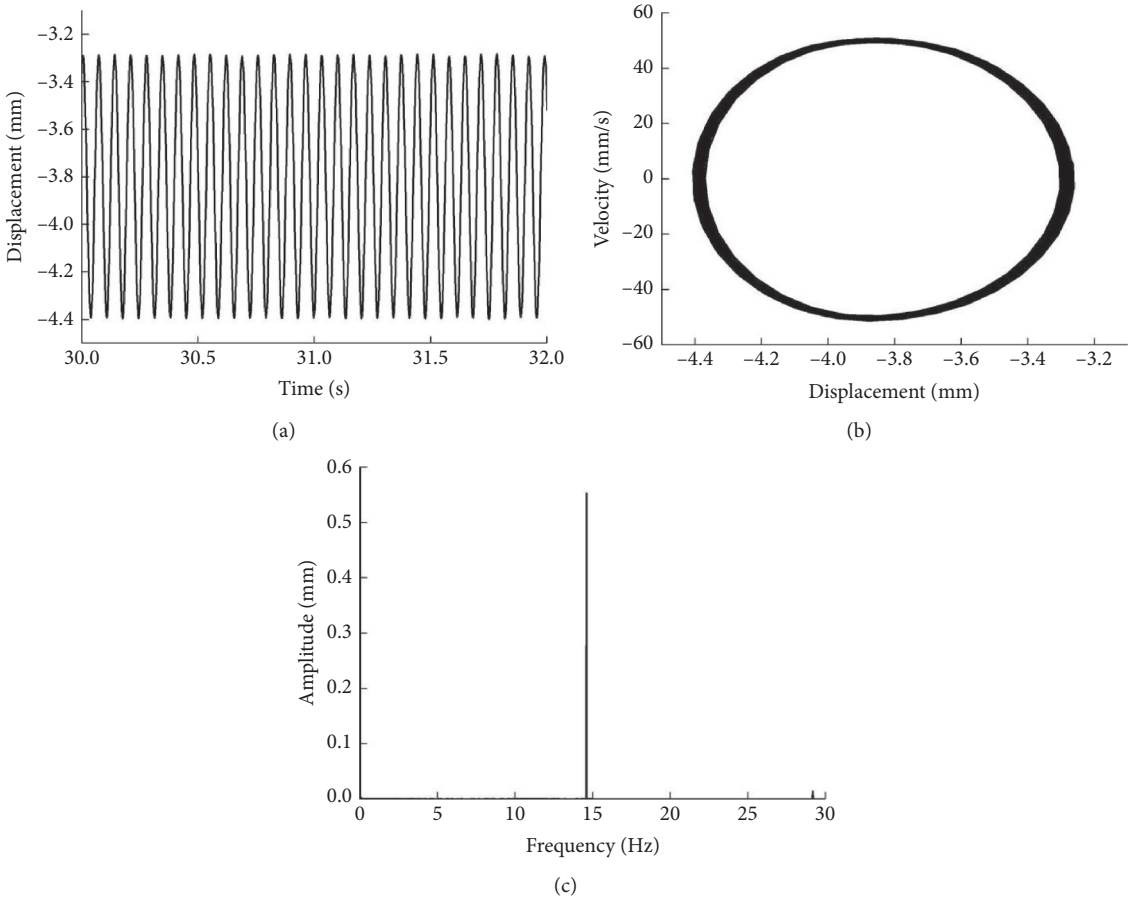

(a)

(b)

(c)

Figure 24: Period-1 motion of the system is obtained for the external excitation frequency $\Omega = 14.6$ Hz: (a) waveform; (b) phase portrait; (c) amplitude spectrum.

motion in vibration of the cantilever beam. Since the vibration amplitude of the chaotic motion becomes small, the output voltage of the system decreases. When the external excitation frequency changes from 12 Hz to 12.2 Hz, the dynamic behavior of the system shows the period-2 motion, as shown in Figure 18. The vibration amplitude of the period-2 motion is larger than that of the chaotic motion. When the external excitation frequency changes from

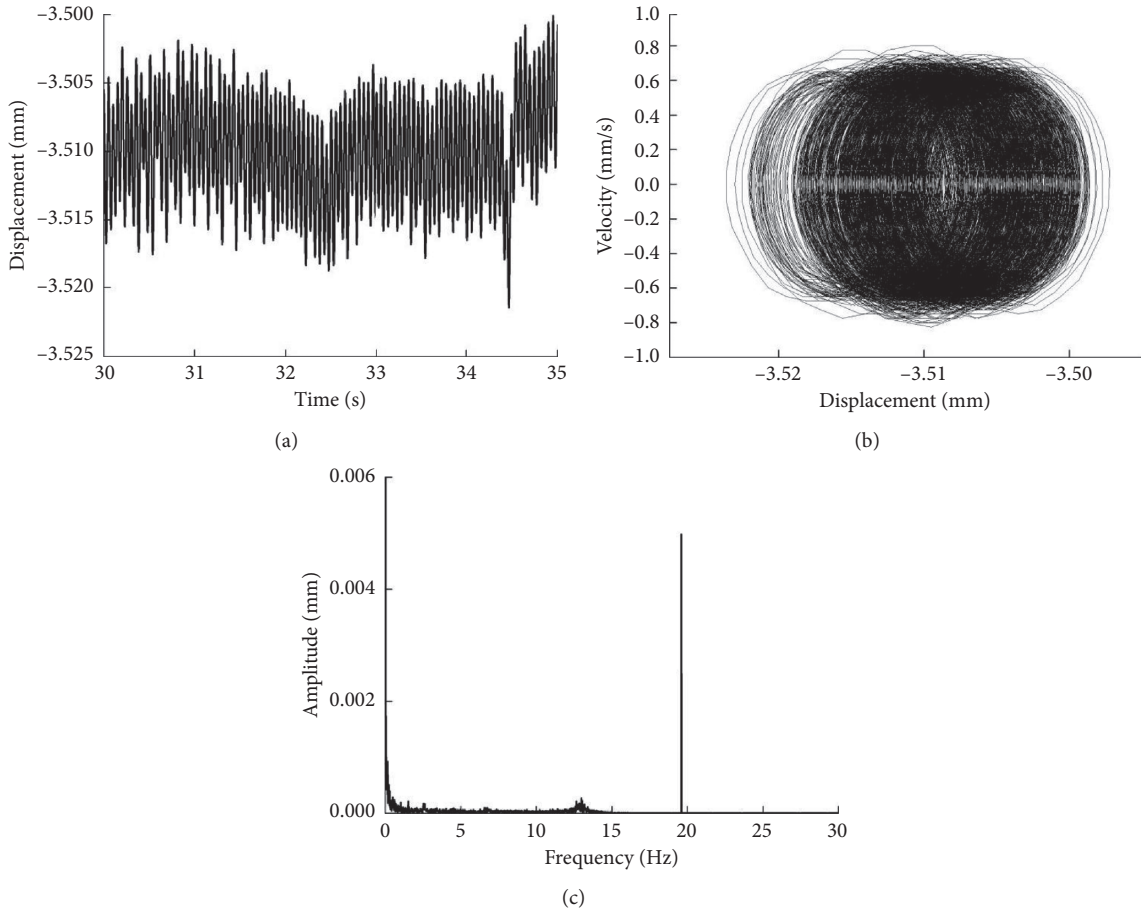

Figure 25: Chaotic motion of the system is obtained for the external excitation frequency $\Omega = 19.6$ Hz: (a) waveform; (b) phase portrait; (c) amplitude spectrum.

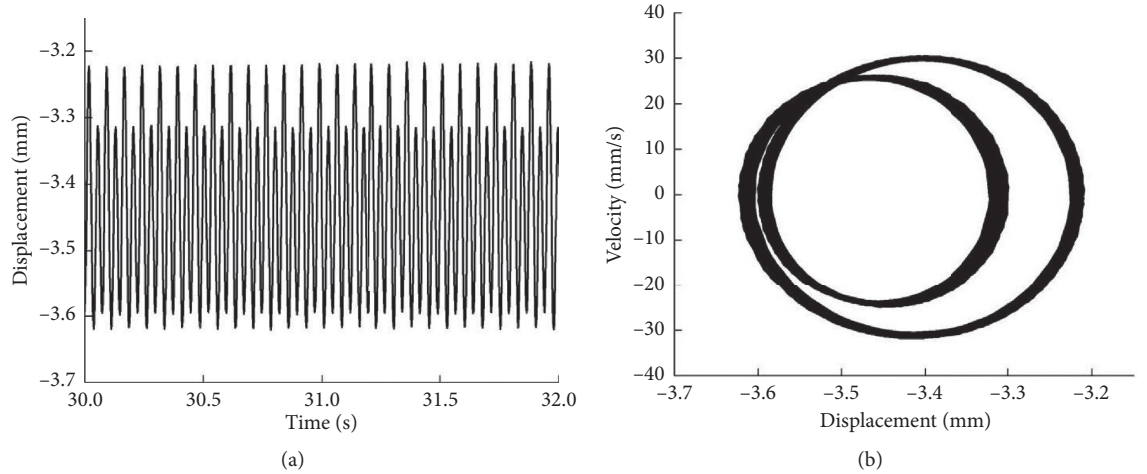

Figure 26: Continued.

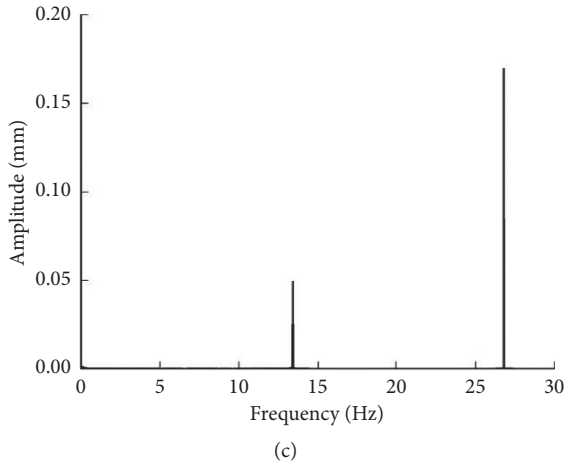

(c)

Figure 26: Period-2 motion of the system is obtained for the external excitation frequency $\Omega = 26.8$ Hz: (a) waveform; (b) phase portrait; (c) amplitude spectrum.

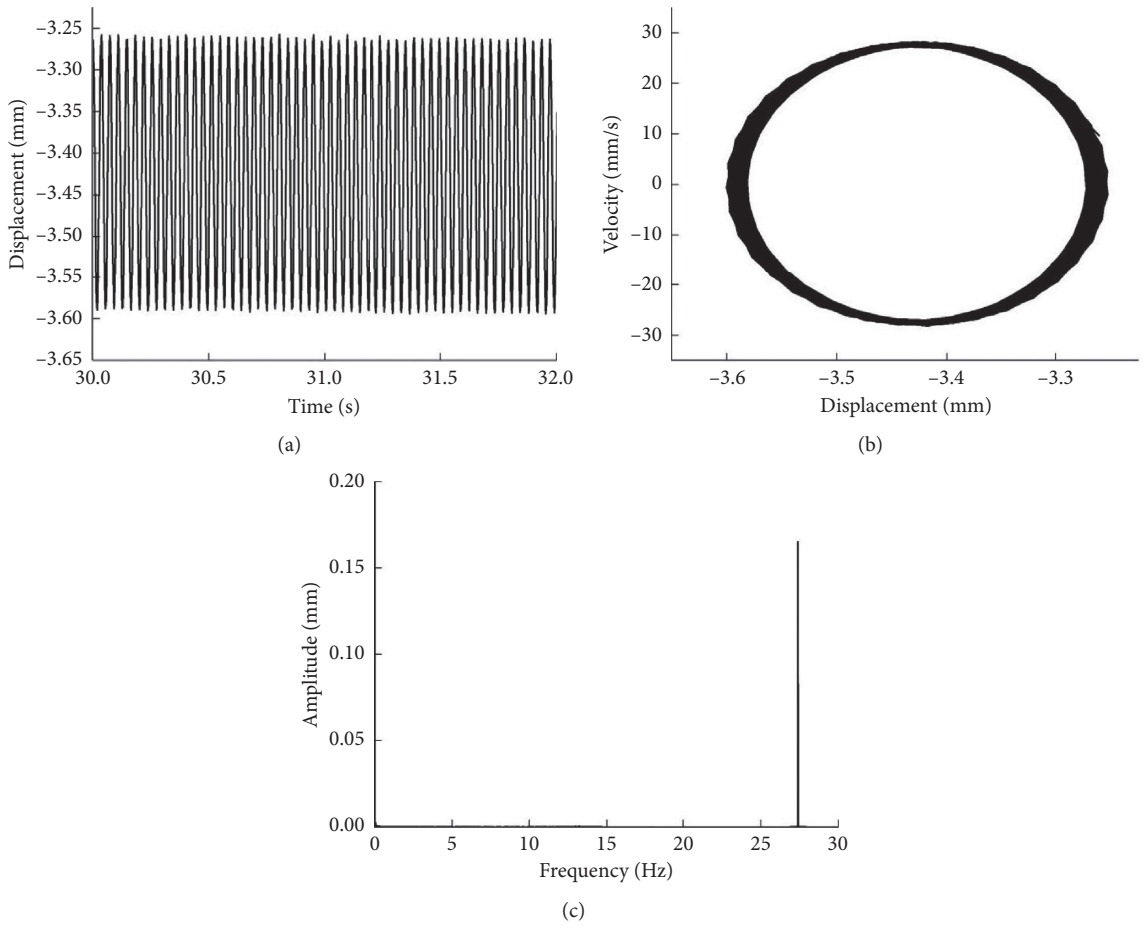

Figure 27: Period-1 motion of the system is obtained for the external excitation frequency $\Omega = 27.4$ Hz: (a) waveform; (b) phase portrait; (c) amplitude spectrum.

12.2 Hz to 12.4 Hz, the dynamic behavior of the system illustrates the multiple period motion, as shown in Figure 19. The vibration amplitude becomes large in the external excitation frequency range of 0.2 Hz. When the external excitation frequency changes from 12.4 Hz to 13 Hz, the dynamic behavior of the chaotic motion is obtained, as

shown in Figure 20. The nonlinear dynamic behavior is obvious, and the piezoelectric cantilever beam continues to vibrate between two stable states. When the external excitation frequency changes from 13 Hz to 13.4 Hz, the dynamic behavior of the system shows the multiple period motion, as shown in Figure 21. When the external excitation frequency changes from 13.4 Hz to 14.2 Hz, the dynamic behavior of the system displays the period-3 motion, as shown in Figure 22. When the external excitation frequency changes from 14.2 Hz to 14.6 Hz, the dynamic behavior of the system demonstrates the quasiperiod motion, as shown in Figure 23. The piezoelectric cantilever beam cannot go through the potential barrier, and the output voltage of the system decreases significantly. According to the above dynamical analysis, it is found that the system can go through the potential barrier to realize the bistable structure at the appropriate frequency range when the magnetic distance is given. The repulsive force between two magnets can be self-tuning by introducing the spring, and the energy going through the potential barrier decreases. The system can vibrate between two stable states, and the output voltage is greater in a wide range of frequencies.

When the external excitation frequency gradually becomes larger, the system can only vibrate in the one stable state. When the external excitation frequency is chosen from 14.6 Hz to 19.6 Hz, the dynamic behavior of the period-1 motion is obtained, as shown in Figure 24. When the external excitation frequency changes from 19.6 Hz to 23 Hz, there is the appearance of the chaotic motion in the system, as shown in Figure 25. When the external excitation frequency changes from 23 Hz to 26 Hz, the dynamic behavior of the system shows the period-1 motion. The vibration amplitude of the system increases slightly, and the output voltage improves slightly.

When the external excitation frequency continues to increase, the piezoelectric cantilever beam vibrates between two stable states again. When the external excitation frequency changes from 26 Hz to 27.4 Hz, the dynamic behavior of the system demonstrates the period-2 motion and the output voltage of the system improves, as shown in Figure 26.

When the external excitation frequency is increased continuously, the system comes back to the one stable state again. When the external excitation frequency changes from 27.4 Hz to 30 Hz, the dynamic behavior of the period-1 motion is obtained, as shown in Figure 27. The vibration amplitude of the cantilever beam is quite small when the external excitation frequency is larger than 30 Hz. The phenomenon of two stable states cannot appear in vibration of the piezoelectric cantilever beam.

According to the above analysis of the experimental results, the law of dynamic behaviors for the system is given as follows: period-1 motion $\longrightarrow$ chaotic motion $\longrightarrow$ period-2 motion $\longrightarrow$ multiple period motion $\longrightarrow$ chaotic motion $\longrightarrow$ multiple period motion $\longrightarrow$ period-3 motion $\longrightarrow$ quasiperiod motion $\longrightarrow$ period-1 motion $\longrightarrow$ -chaotic motion $\longrightarrow$ period-1 motion $\longrightarrow$ period-2 motion $\longrightarrow$ period-1 motion.

When external excitation frequencies are 10.4 Hz, 12 Hz, and 19.6 Hz, respectively, the chaotic motion occurs in vibration of structure C under the case of the magnetic distance of 15 mm. There is the existence of the chaotic motion in structure C under the case of the magnetic distance of 13 mm when the external excitation frequency is 11.8 Hz, 12.4 Hz, and 14 Hz, respectively. The experimental results show that dynamic behaviors of the system are complex when the structure is introduced the spring and the magnet. The bistable phenomenon and the self-tuning magnetic distance are beneficial to broaden the effective frequency bandwidth of the structure.

5.3. Influence of the Magnetic Distance on the Power Generation. The purpose of investigating the magnetic distance is to improve the performance of the multimode power generation device. The problem proposed is whether there is an optimum range of the initial magnetic distances, which make the power generation efficiency of the structure greater. Since the optimum range of the initial magnetic distances exist in the system, the energy through the potential barrier is reduced. The piezoelectric beam easily produces large amplitude vibration between two stable states. In order to obtain an optimum range of the initial magnetic distances, the experiments are conducted under the case of the different magnetic distances. Through further analysis, the optimal initial magnetic distance is found, which makes the power generation efficiency of the system greatest.

In the experiment, the external excitation amplitude is selected as 2.5 V, and the external excitation frequency increases from 5 Hz to 20 Hz. It is obtained from previous experiments that the power generation efficiency of the system is great when the initial magnetic distances are selected from 11 mm to 16 mm. Figure 28 shows that the power generation efficiency of the system is greater when the initial magnetic distances are 13 mm, 14 mm, and 15 mm, respectively. Therefore, the optimum range of the initial magnetic distances is from 13 mm to 15 mm. When the initial magnetic distances are too small, the piezoelectric beam cannot go through the potential barrier, which results in the smaller output voltage. When the initial magnetic distances are too large, it is difficult to realize the bistable structure. The cantilever beam cannot produce large amplitude vibration in a wide range of frequencies. Therefore, the performance of the power generation for the system is improved effectively in an optimum range of the initial magnetic distances.

In the following experiment, the optimal magnetic distance is studied in the optimum range of the initial magnetic distances, which are changed from 11 mm to 16 mm. It is observed from Figure 29 that the optimal initial magnetic distance is 15 mm.

5.4. Optimal External Load of the Structure. In fact, the power generation device is required to connect with the external load. The external load must affect the output power of the system. So, there is the optimal external load, which makes

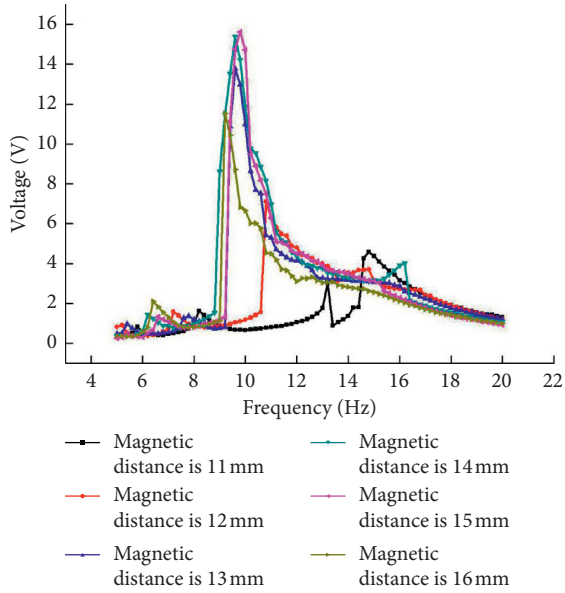

Figure 28: Relation of the voltage-frequency of the structure C is given when initial magnetic distances are selected as 11 mm, 12 mm, 13 mm, 14 mm, 15 mm, and 16 mm, respectively.

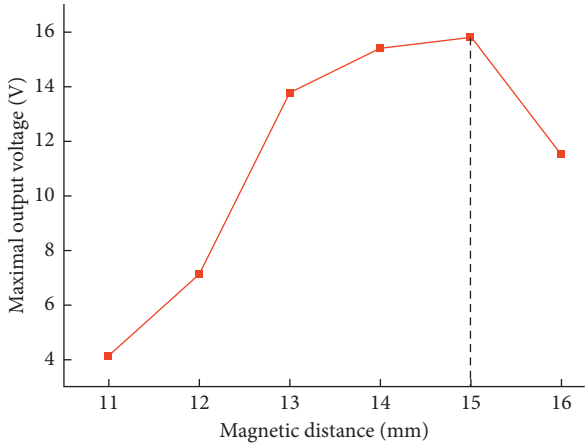

Figure 29: Relation of initial magnetic distances and the maximum output voltage of the structure C.

the output power of the system greatest. In this experiment, the external loads are connected at the end of the generator. The output power of structure C is calculated by measuring the output voltage of each external load. Through the experimental analysis, the optimal external load of the system is obtained.

In the experiment, the external excitation amplitude is 2 V. The external excitation frequency increases from 5 Hz to 30 Hz. Experimental results show that the output power of the system is very low when external loads are less than 1 MΩ, as shown in Figure 30. Firstly, the output power is examined when external loads are 1 MΩ, 3 MΩ, and 5 MΩ, respectively, as shown in Figure 31(a). The output power of the system increases with the increase in external loads. Then, external loads are chosen as 6 MΩ, 8 MΩ, and 10 MΩ. It is shown in Figure 31(b) that the output power of the

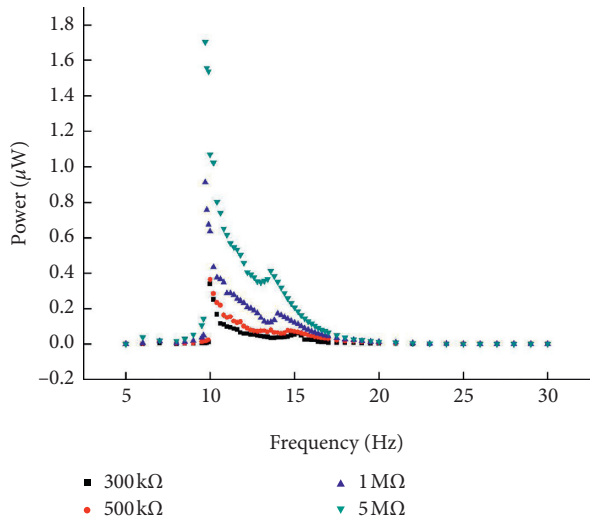

Figure 30: Relation of the power-frequency of the system is given when external loads are selected as 300 kΩ, 500 kΩ, 1 MΩ, and 5 MΩ, respectively.

external load 8 MΩ is greater than that of the external load 6 MΩ. When the external load is 8 MΩ, the output power is maximum. When the external load increases to 10 MΩ, the output power decreases. Figure 31(c) illustrates that the output power of the system decreases with the increase in external loads when external loads of 11 MΩ and 12 MΩ are studied. In order to analyze whether the optimal external load of the system is about 8 MΩ, the output power of the system is further studied when external loads are from 7 MΩ to 9 MΩ. Experimental results show that the output power of the system with the external load of 8 MΩ is the greatest, as shown in Figure 31(d). Based on Figure 31, the conclusion is drawn that the optimal external load of the system is about 8 MΩ. Figure 32 further exhibits the relationship between the output power and the external load of the system.

Based on the above experiment, we have obtained the optimal external load of the system is 8 MΩ. It is further studied whether different initial magnetic distances affect the optimal load of the system. In the experiment, the initial magnetic distances are selected as 12 mm and 15 mm, respectively. The external excitation amplitude of two groups of experiments is both selected as 2 V. It can be seen from Figure 33 that optimal external loads are both 8 MΩ under two different initial magnetic distances. Therefore, the initial magnetic distance cannot have an effect on the optimal external load of the system.

5.5. Influence of Coils on the Power Generation. In the above experiment, the influence of external excitation frequencies, external excitation amplitudes, magnetic distances, and loads on the power generation of the system is studied. In the following experimental investigation, the influence of coils from the electromagnetic induction generator on power generation of the system is examined. The coil is the copper wire. The main parameters of coils include the height, turns, and the wire diameter. Since the power generation efficiency

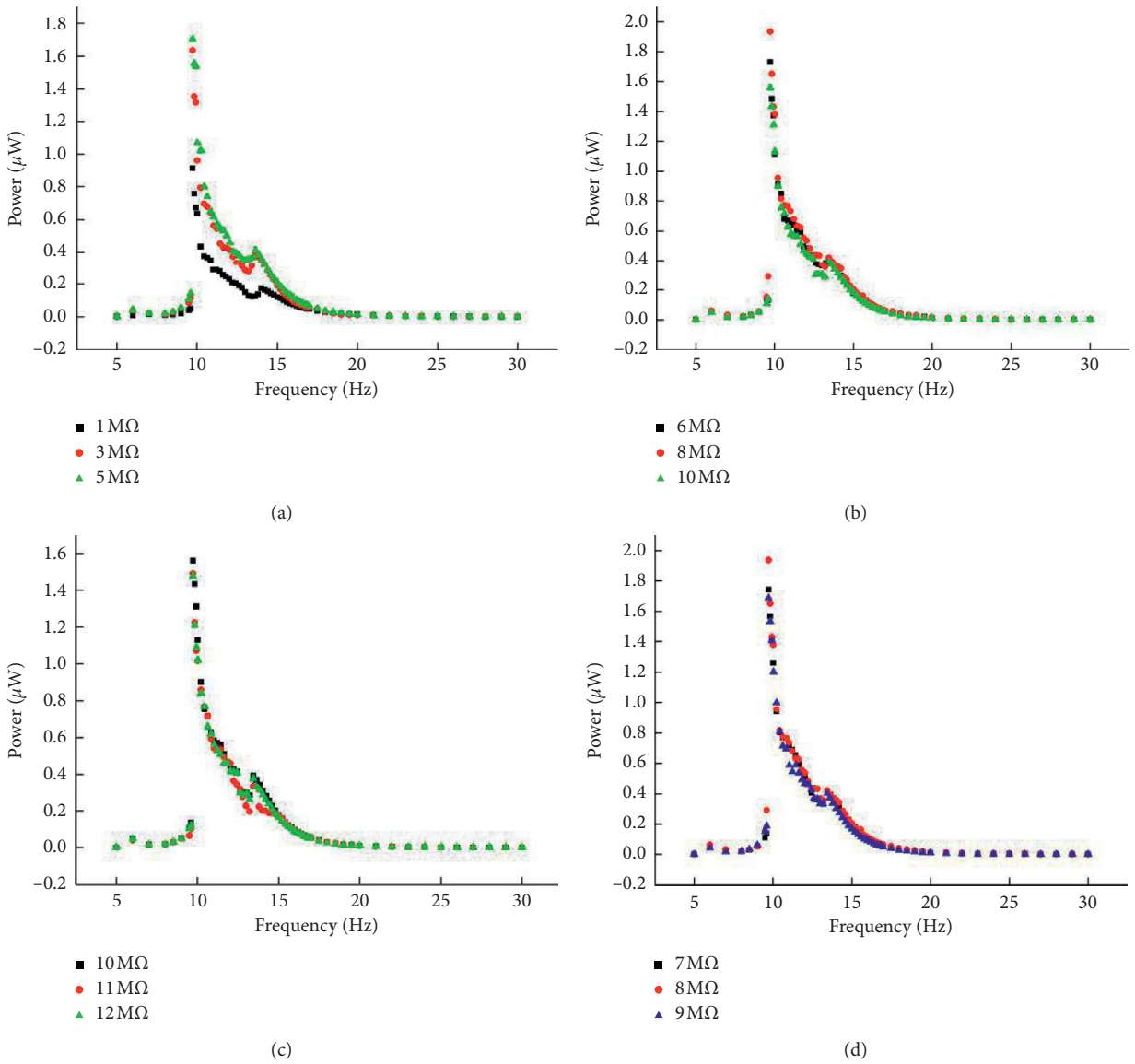

Figure 31: Relation of the power-frequency of different external loads is given: (a) external loads are 1 MΩ,3 MΩ, and 5 MΩ, respectively; (b) external loads are 6 MΩ, 8 MΩ, and 10 MΩ, respectively; (c) external loads are 10 MΩ, 11 MΩ, and 12 MΩ, respectively; (d) external loads are 7 MΩ, 8 MΩ, and 9 MΩ, respectively.

of structure C is the greatest, the influence of parameters of coils on the power generation efficiency of structure C is studied. In the experiment, the external excitation amplitude is selected as 2 V. The influence of heights, turns, and wire diameters of the coil on the power generation efficiency is investigated. Experimental results are shown in Figures 34–37.

In the first step, the influence of the coil height on the power generation efficiency of the system is examined. When the effect of the coil height is studied, the other parameters of coils remain unchanged in the same group of the experiment. The relationship between the output voltage and the external excitation frequency is investigated under the different coil heights. Two different turns of coils are selected to prove that the coil height has a universal effect on power generation of structure C. When turns of coils are selected as 100, Figure 34(a) is obtained. Figure 34(a) demonstrates the comparison of the power generation of the system when heights of coils are selected as 10 mm and 20 mm, respectively. When heights of coils are not changed and turns of coils are chosen as 200, Figure 34(b) is given. It can be obtained from Figures 34(a) and 34(b) that the output voltage of the system, whose the coil height is 10 mm, is greater than that of the system, whose coil height is 20 mm. Therefore, the power generation efficiency of the system decreases when the coil height increases.

Secondly, the influence of the coil turns on the power generation of the system is analyzed, as shown in Figures 35 and 36. The turns of coils are 50 turns, 100 turns, 150 turns, and 200 turns, respectively. The power generation efficiency of the coil of 100 turns is greater than that of the coil of 50 turns, as shown in Figure 35(a). It can be seen from

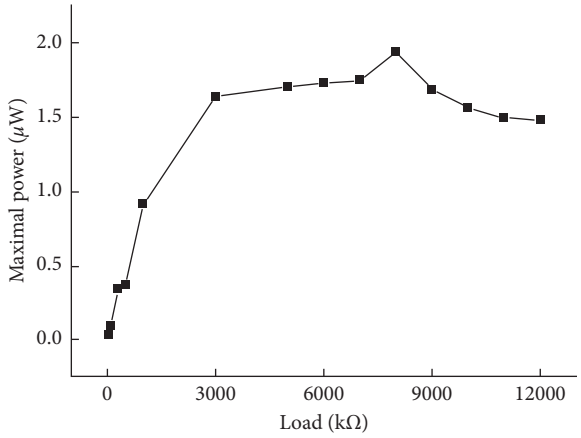

Figure 32: Relation of the maximum power and external loads of the system.

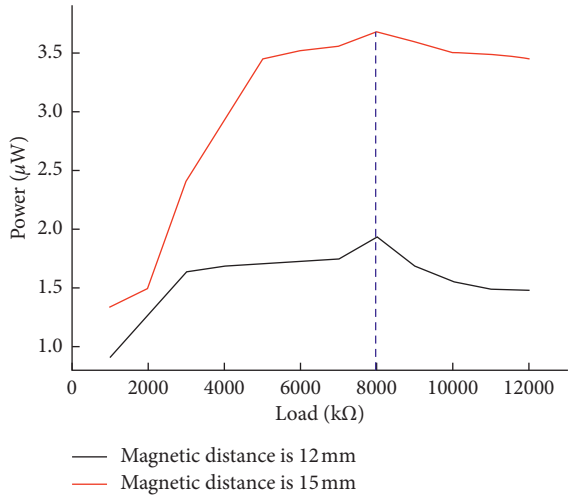

Figure 33: Relation of the power-loads of the system is given when the initial magnetic distances are selected as 12 mm and 15 mm, respectively.

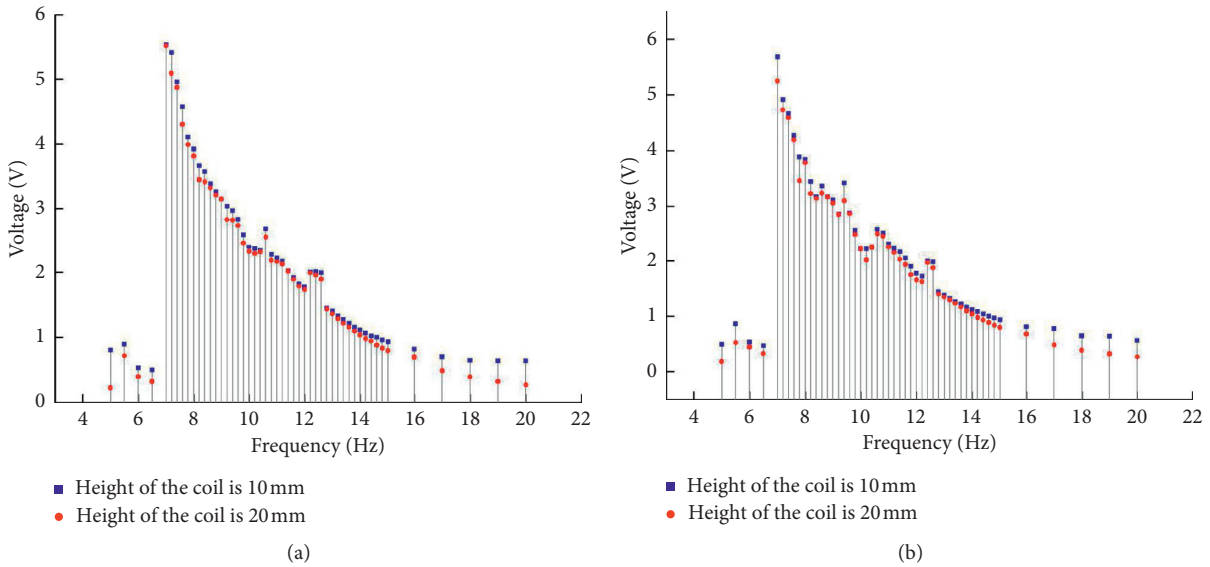

Figure 34: Relation of the voltage-frequency of the system is given when heights of coils are selected as 10 mm and 20 mm, respectively: (a) turns of coils are 100 turns; (b) turns of coils are 200 turns.

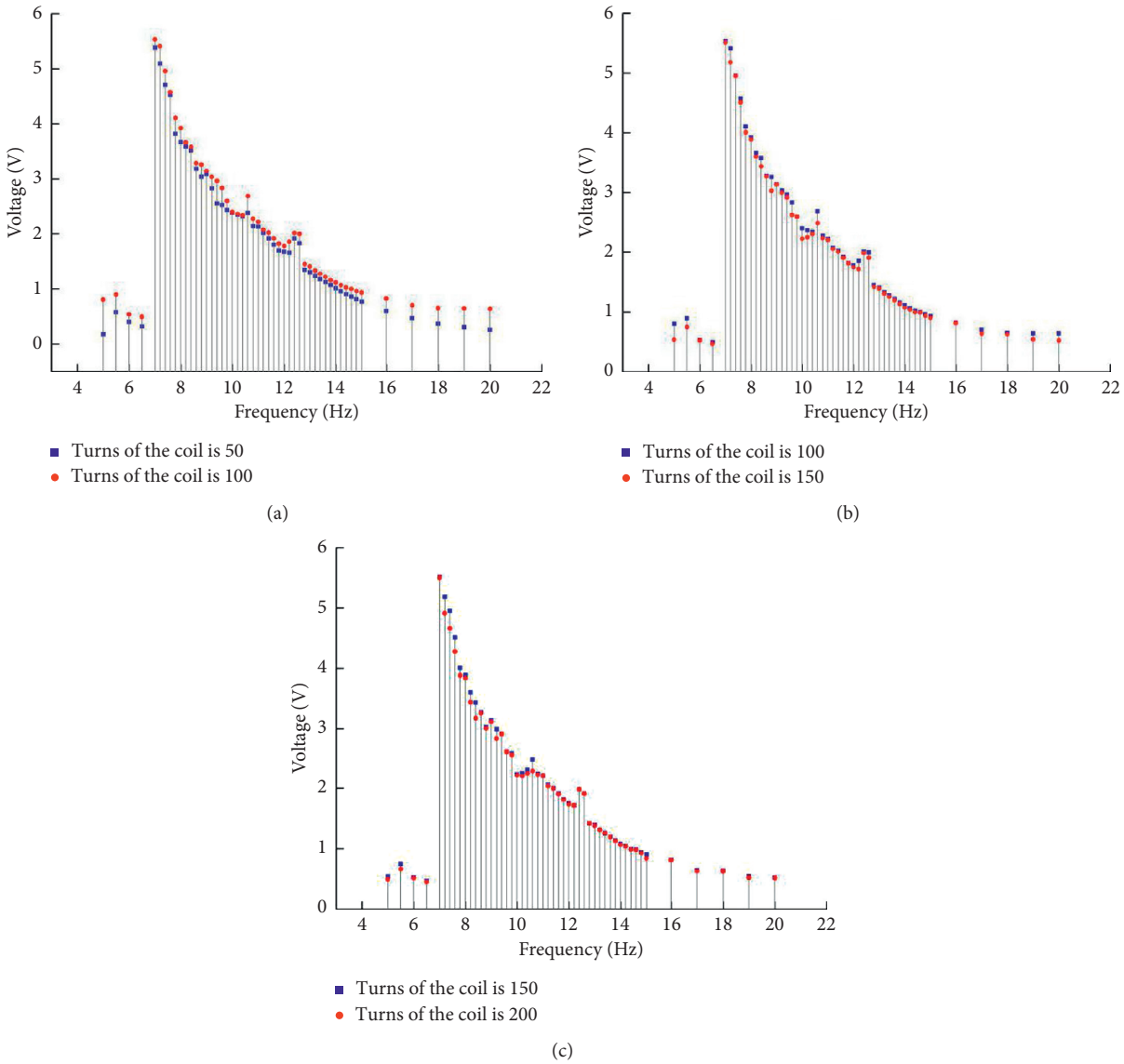

Figure 35: Relation of the voltage-frequency of the system is given when turns of coils are selected as 50, 100, 150, and 200, respectively: (a) coil turns are 50 and 100, respectively; (b) coil turns are 100 and 150, respectively; (c) coil turns are 150 and 200, respectively.

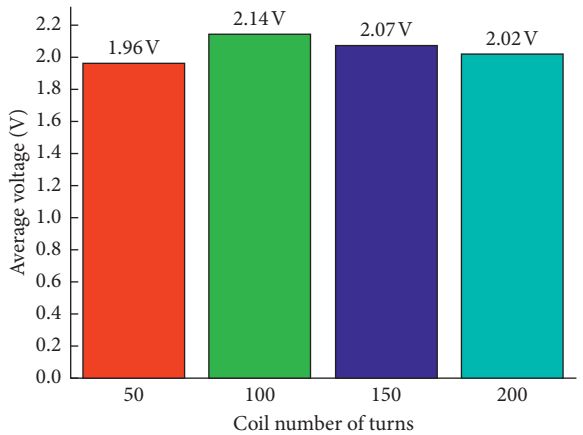

Figure 36: Relation of the average voltage and turns of coils.

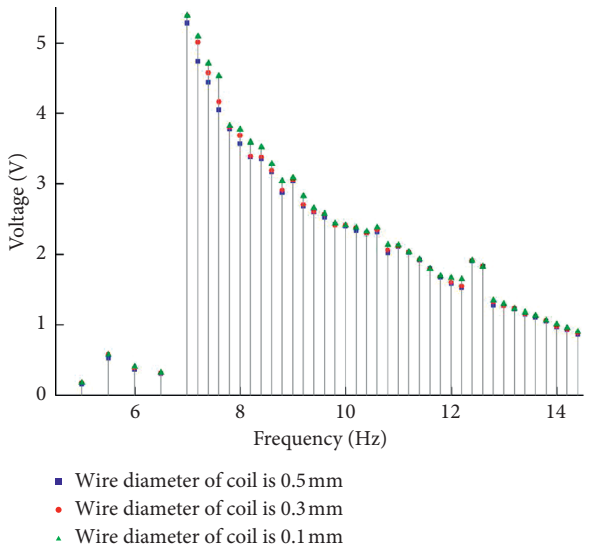

Figure 37: Relation of the voltage-frequency of the system is given when wire diameters of coils are selected as 0.1 mm, 0.3 mm, and 0.5 mm, respectively.

Figure 35(b) that the power generation efficiency of the system decreases when turns of coils increase from 100 turns to 150 turns. It can be obtained from Figure 35(c) that the power generation efficiency of the system decreases when turns of coils increase from 150 turns to 200 turns. Therefore, the power generation efficiency of the system is the greatest when turns of the coil are 100 turns. The result also can be drawn from Figure 36 that the coil has optimal turns, which make the power generation efficiency of the system greatest.

Finally, the influence of wire diameters of the coil on the power generation efficiency of the system is investigated, as shown in Figure 37. The output voltage of the system improves with the decrease in wire diameters of coils. Therefore, the power generation efficiency of the system is improved when wire diameters of coils are increased.

6. Conclusions and Discussion

In this paper, three different kinds of generators are designed: one is the monostable piezoelectric cantilever beam structure (structure A), and other two kinds of structures are bistable piezoelectric cantilever beam structures (structures B and C). The power generation and dynamic behaviors of the different structures are investigated. Following conclusions are drawn:

(1) Comparing the monostable structure with the bistable structure, the power generation of structures B and C is better. The bistable structure is easier to go through the potential barrier by introducing the spring so that the cantilever beam vibrates between two stable states in a wide range of frequencies when the magnetic distance is suitable. When the magnetic distance is very small, the structure produces the larger magnetic force. So, the cantilever beam is difficult to go through the potential barrier, and the nonlinear dynamic behavior is not obvious. When the magnetic distance is too large, the system makes the magnetic force quiet small. The bistable phenomenon of the cantilever beam disappears. Thus, the system improves the output voltage and broadens the effective frequency bandwidth under the condition of the suitable magnetic distance. When the bistable structure is introduced in the electromagnetic power generation, the output voltage of the system can be further improved. Therefore, the power generation of structure C is the best among three kinds of generators.

(2) The power generation capacity of the bistable structure depends on the nonlinear dynamic characteristics of the structure. So, dynamical behaviors of structure C have been studied in detail. The experimental results show that dynamic behaviors of the system are rich and complex when the spring and the magnet are introduced. The repulsive force between two magnets can be self-tuning, and the energy through the potential barrier decreases when the spring is introduced. The system can vibrate between two stable states and the output voltage is greater. The bistable phenomenon and the self-tuning magnetic distance are beneficial to broaden the effective frequency bandwidth of the structure.

(3) The smaller the energy passes through the potential barrier, the greater the power generation efficiency is produced by structure C. Since the magnetic distance affects the energy through the potential barrier, it is needed to find the optimal magnetic distance. In the experiment, the optimum range of the initial magnetic distance and the optimal magnetic distance is investigated in detail. It is found that the optimal initial magnetic distance is 15 mm, which makes the power generation efficiency of the system greatest.

(4) In fact, the power generation of structure C is required to connect with the external load, which can affect the output power of the system. So, there is the optimal external load, which makes the output power of the system greatest. In the experiment, the influence of the external loads on the output power is studied under different initial magnetic distances. It is found that the optimal external load is 8 MΩ. In addition, the initial magnetic distance cannot have an effect on the optimal external load of the system.

(5) Since structure C includes the electromagnetic induction generator, the influence of coils on power generation is needed to further examine. In the experiment, the influence of heights, turns, and wire diameters of the coil on the power generation efficiency is investigated in detail. It is found that the power generation efficiency of the system decreases when heights of coils increase. The optimal turns of coils are found, which makes the power generation efficiency of the system greatest. It is also observed that the wire diameter of the coil is too large to improve the power generation efficiency of the system.

Data Availability

The data used to support the findings of this study are included within the article. Any reader can access the data supporting the conclusions of the study.

Conflicts of Interest

The authors declare that there are no conflicts of interest regarding the publication of this paper.

Acknowledgments

The authors gratefully acknowledge the support of the National Natural Science Foundation of China (NNSFC) (grant nos. 11772008, 11172009, 11372015, 11232009, 10872010, 11290152, and 10732020), Tianjin Natural Science Foundation (grant no. 19JCZDJC32300), and the ASME/IDETC-CIE Conference.

References

[1] S. Roundy, P. K. Wright, and J. Rabaey, "A study of low level vibrations as a power source for wireless sensor nodes," *Computer Communications*, vol. 26, no. 11, pp. 1131–1144, 2003.

[2] E. S. Leland and P. K. Wright, "Resonance tuning of piezoelectric vibration energy scavenging generators using compressive axial preload," *Smart Materials and Structures*, vol. 15, no. 5, pp. 1413–1420, 2006.

[3] S. P. Beeby, M. J. Tudor, and N. M. White, "Energy harvesting vibration sources for microsystems applications," *Measurement Science and Technology*, vol. 17, no. 12, pp. 175–195, 2006.

[4] B. P. Mann and B. A. Owens, "Investigations of a nonlinear energy harvester with a bistable potential well," *Journal of Sound and Vibration*, vol. 329, no. 9, pp. 1215–1226, 2009.

[5] S. C. Stanton, C. C. McGehee, and B. P. Mann, "Nonlinear dynamics for broadband energy harvesting: investigation of a bistable piezoelectric inertial generator," *Physica D: Nonlinear Phenomena*, vol. 239, no. 10, pp. 640–653, 2010.

[6] A. Erturk and D. J. Inman, "Broadband piezoelectric power generation on high-energy orbits of the bistable duffing oscillator with electromechanical coupling," *Journal of Sound and Vibration*, vol. 330, no. 10, pp. 2339–2353, 2010.

[7] M. Ferrari, V. Ferrari, M. Guizzetti, B. Andò, S. Baglio, and C. Trigona, "Improved energy harvesting from wideband vibrations by nonlinear piezoelectric converters," *Sensors and Actuators A: Physical*, vol. 162, no. 2, pp. 425–431, 2010.

[8] H. A. Ma, J. Q. Liu, G. Tang, C. S. Yang, and Y. G. Li, "A magnetic structure for broadband piezoelectric vibration energy harvester," *Transducer and Micro-system Technologies*, vol. 30, no. 4, pp. 66–68, 2011.

[9] A. F. Arrieta, T. Delpero, A. E. Bergamini, and P. Ermanni, "Broadband vibration energy harvesting based on cantilevered piezoelectric bi-stable composites," *Applied Physics Letters*, vol. 102, no. 17, Article ID 173904, 2013.

[10] W. Al-Ashtari, M. Hunstig, T. Hemsel, and W. Sextro, "Increasing the power of piezoelectric energy harvesters by magnetic stiffening," *Journal of Intelligent Material Systems and Structures*, vol. 24, no. 11, pp. 1332–1342, 2013.

[11] E. K. Ali and J. Kyle, "Efficiency enhancement of a cantilever-based vibration energy harvester," *Sensors*, vol. 14, pp. 188–211, 2014.

[12] K. Fan, J. Chang, F. Chao, and W. Pedrycz, "Design and development of a multipurpose piezoelectric energy harvester," *Energy Conversion and Management*, vol. 96, pp. 430–439, 2015.

[13] M. H. Yao, W. Zhang, and Z. G. Yao, "Nonlinear vibrations and chaotic dynamics of the laminated composite piezoelectric beam," *Journal of Vibration and Acoustics*, vol. 137, no. 1, Article ID 011002, 2015.

[14] A. Jemai, F. Najar, M. Chafra, and Z. Ounaies, "Modeling and parametric analysis of a unimorph piezocomposite energy harvester with interdigitated electrodes," *Composite Structures*, vol. 135, pp. 176–190, 2016.

[15] S. Arkadiusz, R. B. Christopher, H. A. Kim, R. Andrzej, and L. Grzegorz, "Responses of bistable piezoelectric-composite energy harvester by means of recurrences," *Mechanical Systems and Signal Processing*, vol. 76-77, pp. 823–832, 2016.

[16] X. D. Xie and Q. Wang, "A study on a high efficient cylinder composite piezoelectric energy harvester," *Composite Structures*, vol. 161, pp. 237–245, 2017.

[17] T. Galchev, H. Kim, and K. Najafi, "Micro power generator for harvesting low-frequency and nonperiodic vibrations," *Journal of Microelectromechanical System*, vol. 20, no. 4, pp. 852–866, 2011.

[18] I. Sari, T. Balkan, and H. Kulah, "An electromagnetic micro power generator for wideband environmental vibrations," *Sensors and Actuators*, vol. 11, pp. 1–9, 2007.

[19] B. P. Mann and N. D. Sims, "Energy harvesting from the nonlinear oscillations of magnetic levitation," *Journal of Sound and Vibration*, vol. 319, no. 1-2, pp. 515–530, 2009.

[20] E. Sardini and M. Serpelloni, "An efficient electromagnetic power harvesting device for low-frequency applications," *Sensors and Actuators A-Physical*, vol. 172, no. 2, pp. 475–482, 2010.

[21] Ö. Zorlu, E. T. Topal, and H. Kulah, "A vibration-based electromagnetic energy harvester using mechanical frequency up-conversion method," *IEEE Sensors Journal*, vol. 11, no. 2, pp. 481–488, 2011.

[22] A. R. M. Foisal, C. Hong, and G.-S. Chung, "Multi-frequency electromagnetic energy harvester using a magnetic spring cantilever," *Sensors and Actuators A: Physical*, vol. 182, pp. 106–113, 2012.

[23] R. Ramlan, M. J. Brennan, B. R. Mace, and S. G. Burrow, "On the performance of a dual-mode non-linear vibration energy harvesting device," *Journal of Intelligent Material Systems and Structures*, vol. 23, no. 13, pp. 1423–1432, 2012.

[24] D. Kremer and K. Liu, "A nonlinear energy sink with an energy harvester: transient responses," *Journal of Sound and Vibration*, vol. 333, no. 20, pp. 4859–4880, 2014.

[25] M.-L. Seol, J.-W. Han, S.-J. Park, S.-B. Jeon, and Y. K. Choi, "Hybrid energy harvester with simultaneous triboelectric and electromagnetic generation from an embedded floating oscillator in a single package," *Nano Energy*, vol. 23, pp. 50–59, 2016.

[26] M. Resali and H. Salleh, "Comparison of an electromagnetic energy harvester performance using wound coil wire and PCB coil," *Earth and Environmental Science*, vol. 32, Article ID 012059, 2016.

[27] T. Wacharasindhu and J. W. Kwon, "A micromachined energy harvester from a keyboard using combined electromagnetic and piezoelectric conversion," *Journal of*

Micromechanics and Microengineering, vol. 18, no. 10, Article ID 104016, 2008.

[28] Y. Tadesse, S. J. Zhang, and S. Priya, "Multimodal energy harvesting system: piezoelectric and electromagnetic," *Journal of Intelligent Material Systems and Structures*, vol. 20, no. 5, pp. 625–632, 2009.

[29] V. R. Challa, M. G. Prasad, and F. T. Fisher, "A coupled piezoelectric electromagnetic energy harvesting technique for achieving increased power output through damping matching," *Smart Materials and Structures*, vol. 18, Article ID 095029, 2009.

[30] M. A. Karami and D. J. Inman, "Nonlinear hybrid energy harvesting utilizing piezo-magneto-elastic spring," in *Proceedings of the 2010 Conference on Active and Passive Smart Structures and Integrated Systems*, San Diego, CA, USA, March 2010.

[31] B. Yang, C. K. Lee, W. L. Kee, and S. P. Lim, "Hybrid energy harvester based on piezoelectric and electromagnetic mechanisms," *Journal of Micro/Nanolithography, MEMS, and MOEMS*, vol. 9, no. 2, Article ID 023002, 2010.

[32] H.-y. Wang, L.-h. Tang, Y. Guo, X.-b. Shan, and T. Xie, "A 2DOF hybrid energy harvester based on combined piezoelectric and electromagnetic conversion mechanisms," *Journal of Zhejiang University SCIENCE A*, vol. 15, no. 9, pp. 711–722, 2014.

[33] S. Mahmoudi, N. Kacem, and N. Bouhaddi, "Enhancement of the performance of a hybrid nonlinear vibration energy harvester based on piezoelectric and electromagnetic transductions," *Smart Materials and Structures*, vol. 23, no. 7, Article ID 075024, 2014.

[34] R. Hamid and M. R. Yuce, "A wearable energy harvester unit using piezoelectric-electromagnetic hybrid technique," *Sensors and Actuators A: Physical*, vol. 257, pp. 198–207, 2017.

[35] M. H. Yao, L. Ma, and W. Zhang, "Study on power generations and dynamic responses of the bistable straight beam and the bistable L-shaped beam," *Science China Technological Sciences*, vol. 61, no. 9, pp. 1404–1416, 2018.

[36] M. H. Yao, P. F. Liu, L. Ma, H. B. Wang, and W. Zhang, "Experimental study on broadband bistable energy harvester with L-shaped piezoelectric cantilever beam," *Acta Mechanica Sinica*, vol. 36, no. 3, pp. 557–577, 2020.

[37] M. H. Yao, P. F. Liu, W. Zhang, and D. X. Cao, "The experimental study on a bistable piezoelectric-electromagnetic combined vibration energy harvester," in *Proceedings of the ASME International Design Engineering Technical Conferences and Computers and Information in Engineering Conference (IDETC/CIE 2017)*, Cleveland, OH, USA, August 2017.

[38] M. Getzlaff, *Fundamentals of Magnetism*, Springer, Berlin, Germany, 2008.